iScience

CellPress
OPEN ACCESS

Article

Zfp521 is essential for the quiescence and maintenance of adult hematopoietic stem cells under stress

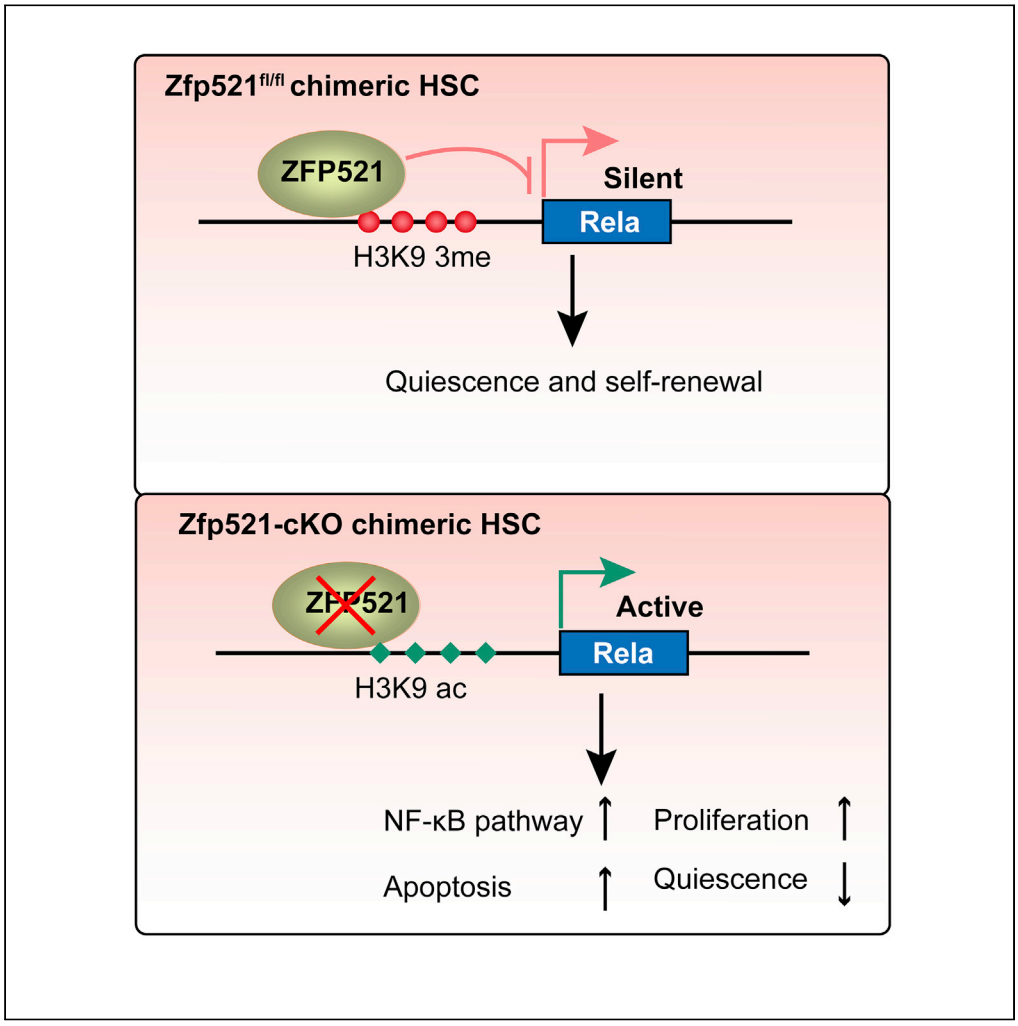

Zhigang Li, Xuemei Fu, Weiru Wu, ..., Guangling Zheng, Jieping Chen, Yu Hou

chenjpxn@163.com (J.C.)
houyuxn@vip.126.com (Y.H.)

HIGHLIGHTS

Zfp521 deletion does not inhibit adult hematopoiesis under homeostatic conditions

Zfp521 regulates the quiescence and maintenance of HSC under stress

Zfp521 deficiency affects the NF-κB pathway in HSC

Knockdown of *Rela* reverses the loss of quiescence in Zfp521-null HSC under stress

Li et al., iScience *24*, 102039
February 19, 2021
https://doi.org/10.1016/j.isci.2021.102039

iScience

CellPress
OPEN ACCESS

Article

Zfp521 is essential for the quiescence and maintenance of adult hematopoietic stem cells under stress

Zhigang Li,[1] Xuemei Fu,[1] Weiru Wu,[1] Zhilong Liu,[1] Zhe Chen,[1] Chengfang Zhou,[1] Yuanyuan Liu,[1] Mei Kuang,[1] Fangfang Sun,[1] Feifei Xiao,[1] Yongxiu Huang,[1] Xiaojun Zhang,[1] Shijun Fan,[2] Xingqin Huang,[1] Guangling Zheng,[3] Jieping Chen,[1,*] and Yu Hou[1,4,*]

SUMMARY

Zinc finger protein 521 (*Zfp521*), a quiescent hematopoietic stem cell (HSC)-enriched transcription factor, is involved in the self-renewal and differentiation of fetal liver HSC. However, its role in adult hematopoiesis remains elusive. Here, we found that *Zfp521* deletion did not inhibit adult hematopoiesis under homeostatic conditions. In contrast, *Zfp521*-null chimeric mice showed significantly reduced pool size of HSC and hematopoietic progenitor cells associated with increased apoptosis and loss of quiescence. Competitive serial transplantation assays revealed that *Zfp521* regulates HSC self-renewal and differentiation under regenerative stress. Mechanistically, *Zfp521* transcriptionally repressed *Rela* expression by increasing H3K9ac and decreasing H3K9me3 levels in its promoter. Knockdown of *Rela* inhibited the hyper-activated NF-κB pathway and reversed the loss of quiescence in *Zfp521*-null HSC under stress. Thus, our results reveal a previously unrecognized role for *Zfp521* as critical regulator of quiescence and self-renewal of HSC in adult hematopoiesis mediated at least partly by controlling *Rela* expression.

INTRODUCTION

Mammalian definitive hematopoiesis is a complex and finely regulated process in which hematopoietic stem cells (HSCs) give rise to all blood lineages of the organism including fetal liver and adult hematopoiesis during ontogeny (Dzierzak and Speck, 2008). The corresponding fetal liver and adult HSC are regulated by distinct intrinsic and extrinsic mechanisms (Wilkinson et al., 2020). In adult hematopoiesis, HSC mainly resides in the bone marrow (BM) niche and remains quiescent in a steady state. However, HSC can exit quiescence, and rapidly expand and differentiate to reconstitute the hematopoietic system under stress such as blood loss (Enver et al., 1998) and myelotoxic insults (Cheshier et al., 1999). The balance between quiescence and proliferation is tightly regulated by both intrinsic and extrinsic mechanisms in HSC under stress but the precise mechanisms remain to be fully elucidated. A better understanding of how these processes are regulated could lead to improved strategies for the clinical utility of HSC and provide insight into the basis of hematopoietic malignancy.

Zinc finger protein 521 (human, *ZNF521*; mouse, *Zfp521*) is a C2H2-type zinc finger transcription factor containing a conserved amino terminal motif that binds to the nucleosome remodeling and histone deacetylase complex (NuRD), which is associated with transcriptional repression (Lin et al., 2004). *ZNF521* was initially identified as having restricted expression in human $CD34^+$ progenitor cells (Bond et al., 2004); however, it is widely expressed in many tissues where it regulates self-renewal and differentiation. *Zfp521* negatively modulates differentiation by repressing ZFP432, EBF1, and RUNX2 (Addison et al., 2014; Kang et al., 2012b; Wu et al., 2009) and negatively regulates apoptosis via BCL-2 in mesenchymal stem cells (Correa et al., 2010). A forced expression of *Zfp521* in embryonic stem cells led to a skewed differentiation toward a self-renewing neural progenitor cell fate (Kamiya et al., 2011; Shahbazi et al., 2016). In the hematopoietic system, *ZNF521/Zfp521* is expressed in early HSC and absent in mature cells (Bond et al., 2004). *Zfp521* contributes to maintaining the multipotency of primitive lympho-myeloid progenitors by inhibiting EBF1-driven commitment toward the B-cell lineage (Mega et al., 2011). ZFP521 inhibits erythroid differentiation in leukemia cell lines through direct binding with GATA-1 and inhibiting its activity (Matsubara et al., 2009). Garrison BS first reported that $Zfp521^{-/-}$ HSC derived from fetal liver exhibited marked decrease in HSC frequency after two rounds of competitive serial transplantation, suggesting that *Zfp521* regulates HSC self-renewal ability *in vivo* (Garrison et al., 2017). *Zfp521* regulates the earliest stages of

[1]Department of Hematology, Southwest Hospital, Third Military Medical University (Army Medical University), Chongqing 400038, China

[2]Medical Research Center, Southwest Hospital, Third Military Medical University (Army Medical University), Chongqing 400038, China

[3]Department of Radiology, Southwest Hospital, Third Military Medical University (Army Medical University), Chongqing 400038, China

[4]Lead contact

*Correspondence: chenjpxn@163.com (J.C.), houyuxn@vip.126.com (Y.H.)

https://doi.org/10.1016/j.isci.2021.102039

hematopoiesis and lymphoid cell development via a cell-extrinsic mechanism using the whole-body knockout (KO) mouse model (Fleenor et al., 2018). Given that *Zfp521*$^{-/-}$ mice die within a few weeks of birth, the molecular mechanisms underlying its regulation of adult HSC function are yet to be fully characterized.

Herein, we investigated the function of *Zfp521* in hematopoietic stem and progenitor cells (HSPCs) using conditional KO mouse models with loss of *Zfp521* specifically in hematopoietic systems. We found that *Zfp521* deficiency decreased the frequency of quiescent HSC and increased the proliferation of HSPC under stress. Consequently, the self-renewal capacity of *Zfp521*-deficient HSC was significantly lower than that of *Zfp521*-sufficient HSC in chimeric mice. Mechanistically, loss of *Zfp521* induced downregulation of cyclin-dependent kinase inhibitors, including p21 and p57, by directly upregulating the expression of *Rela*, a critical effector of NF-κB pathway and crucial regulator of HSC quiescence (Nakagawa et al., 2018; Stein and Baldwin, 2013). Thus, our data indicated that *Zfp521* is a critical regulator of the quiescence and self-renewal capacity of HSC through *Rela*-mediated NF-κB pathways.

RESULTS

Generation of *Zfp521* conditional KO mice

To the best of our knowledge, there are no reports on the cell-intrinsic regulation of adult hematopoiesis by *Zfp521*. To assess the role of *Zfp521* in adult HSPC we first determined the expression level of *Zfp521* in subsets of primitive and mature BM cells. Real-time polymerase chain reaction (RT-PCR) revealed that *Zfp521* was highly enriched in HSC, especially in quiescent HSC, compared to progenitors and differentiated cells (Figure 1A), suggesting an important role of *Zfp521* in HSC.

Since *Zfp521*$^{-/-}$ mice die within a few weeks of birth (Kiviranta et al., 2013), we generated a Zfp521 conditional KO allele (*Zfp521*$^{fl/+}$) by inserting two *loxP* sites flanking *Zfp521* exon4, which encodes around 85% of the amino acids of *Zfp521*. Deletion of exon4 could also result in a frameshift and trigger nonsense-mediated decay of the mutant mRNA transcript (Figure 1B). To investigate the function of *Zfp521* in adult hematopoiesis, we generated inducible conditional KO mice (*Zfp521*$^{fl/fl}$*Mx1-Cre*) by crossing mice carrying a *loxP*-flanked (floxed) copy of the gene (*Zfp521*$^{fl/fl}$) with mice carrying the *Mx1-Cre* driver. Conditional deletion of *Zfp521* was induced in *Zfp521*$^{fl/fl}$*Mx1-Cre* mice by three intraperitoneal injections of polyinosinic-polycytidylic acid (pIpC) (called "*Zfp521*-CKO mice" here). Control mice throughout this study (unless specified otherwise) consisted of *Zfp521*$^{fl/fl}$ littermates that were treated identically to experimental mice, including receiving injections of pIpC to control for interferon-mediated effects (Baldridge et al., 2010). Two months after pIpC induction, we confirmed a high efficiency of *Zfp521* deletion in Lin^{-}Sca-1^{+}c-Kit^{+} (LSK) cells by semiquantitative PCR analysis of genomic DNA isolated from LSK cells from *Zfp521*-CKO mice (Figure 1C). Accordingly, real-time PCR analysis showed only trace amounts of *Zfp521* mRNA in BM and LSK cells from *Zfp521*-CKO mice (Figures 1D and 1E).

Zfp521 loss has no effect on adult hematopoiesis under homeostatic conditions

At 2 months of age, *Zfp521*$^{fl/fl}$*Mx1-Cre* mice and the littermate controls were administered three intraperitoneal injections of pIpC at a dosage of 8–10 mg/kg every second day. Two months after pIpC induction, *Zfp521*-CKO mice developed normal white blood cells (WBCs), red blood cells (RBCs), platelet counts, and hemoglobin (Hb) levels in the peripheral blood (PB) compared with control littermates (Figure 1F and Table S1). Analysis of the lineage distributions in the BM, spleen, and thymus from *Zfp521*-CKO mice and control littermates by cytometric analysis revealed that *Zfp521*-CKO mice had a normal frequency of myeloid cells, B cells, T cells, and RBC in these tissues (Figures S1A–S1C). The absolute number of long-term HSC (LT-HSC), short-term HSC (ST-HSC), multipotent progenitors (MPPs), LSK cells, HPC, common myeloid progenitors (CMPs), granulocyte/macrophage progenitors (GMPs), and megakaryocyte/erythroid progenitors (MEPs) in the BM of *Zfp521*-CKO mice was also comparable to that in *Zfp521*$^{fl/fl}$ mice (Figures 2A and 2B). Furthermore, in the steady state, no significant difference was observed in the cell cycle and quiescence status of *Zfp521*-CKO HSC compared to that of *Zfp521*$^{fl/fl}$ HSC (Figures 2C and 2D). These results suggest that *Zfp521* loss did not interfere with adult hematopoiesis under the steady state.

Depletion of *Zfp521* impairs the size of HSC pools after transplantation

Although the expression of *Zfp521* was higher in HSC than in differentiated cells, *Zfp521* loss did not affect HSC number and proliferation in the homeostatic state. This prompted us to test the role of *Zfp521* in HSC under stress. BM transplantation exposes HSC to replicative, oxidative, and inflammatory stresses (Baldridge

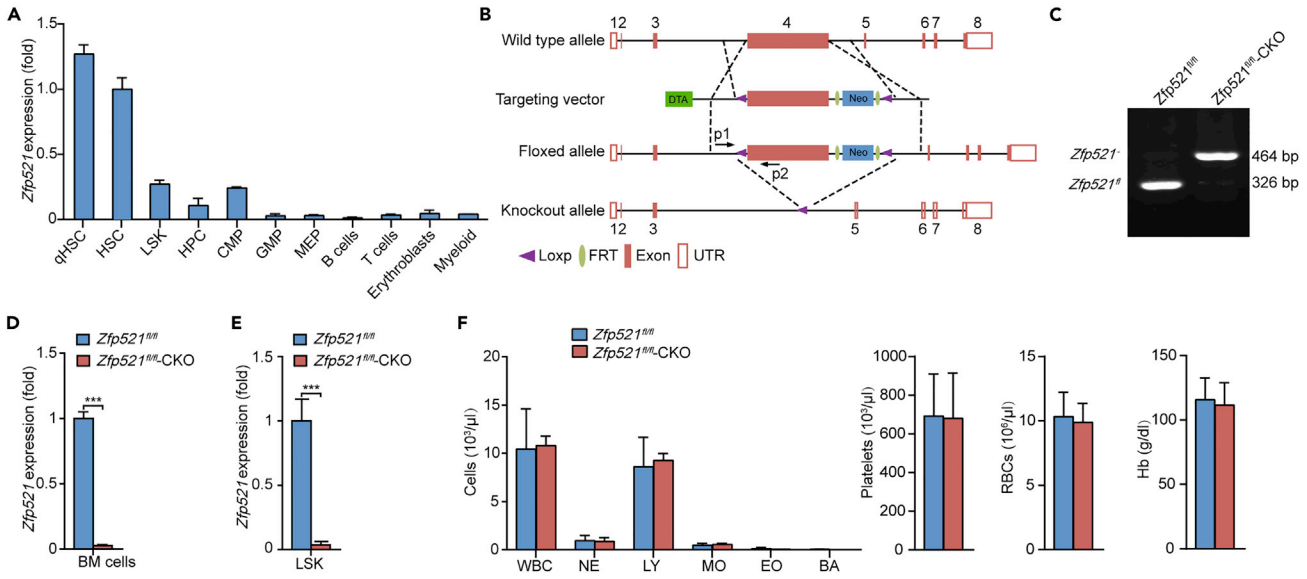

Figure 1. *Zfp521* loss does not alter adult hematopoiesis under homeostatic conditions

(A) Quantitative RT-PCR analysis of *Zfp521* in hematopoietic cells from wild-type BM; results were normalized to expression of the control gene *Actb* and are presented relative to those of HSC, set as 1. The distinct subsets of primitive or mature cells were sorted by indicated cell surface markers: qHSC indicates quiescent HSC, Lin$^-$Sca-1$^+$c-Kit$^+$CD48$^-$CD150$^+$Pyronin Y$^-$; HSC, Lin$^-$Sca-1$^+$c-Kit$^+$CD48$^-$CD150$^+$; LSK, Lin$^-$Sca-1$^+$c-Kit$^+$; HPC, Lin$^-$Sca-1$^-$c-Kit$^+$; CMP, Lin$^-$Sca-1$^-$c-Kit$^+$CD34$^+$CD16/32$^-$; GMP, Lin$^-$Sca-1$^-$c-Kit$^+$CD34$^+$CD16/32$^+$; MEP, Lin$^-$Sca-1$^-$c-Kit$^+$CD34$^-$CD16/32$^-$; B cells, B220$^+$; T cells, CD4$^+$ or CD8$^+$; Erythroblasts, CD71$^+$Ter119$^+$; Myeloid, Mac-1$^+$Gr-1$^+$.

(B) Schematic representation of the targeting strategy of *Zfp521*. *Zfp521* locus, the targeting vector, floxed allele, and the KO loci. Exon 4 was flanked by *loxP* sites and a neomycin resistance gene (*Neo*) was inserted after exon 4, which generated *Zfp521*$^{fl/fl}$ mice. *Zfp521*$^{fl/fl}$ alleles were combined with *Mx1-Cre* to generate *Zfp521*$^{fl/fl}$; *Mx1-Cre* in which *Zfp521* is specifically deleted in the hematopoietic system induced by intraperitoneal injections of poly (I:C). The targeting vector contained a diphtheria toxin fragment A (*DTA*) and *Neo* genes. The arrows indicate the position and direction of primers used for genotyping.

(C) Semiquantitative PCR analysis of the deletion of *Zfp521*(*Zfp521*$^-$) and the *lox*P-flanked *Zfp521* allele (*Zfp521*^{fl}) among genomic DNA in BM LSK cells from *Zfp521*$^{fl/fl}$ and *Zfp521*-CKO mice. Molecular sizes are indicated in base pairs (bp).

(D and E) Quantitative RT-PCR analysis of *Zfp521* mRNA in BM cells (D) or LSK cells (E) from *Zfp521*$^{fl/fl}$ and *Zfp521*-CKO mice; *Actb* was used as an internal control and results are presented relative to those of HSC in *Zfp521*$^{fl/fl}$.

(F) Absolute number of WBC, neutrophils (NEs), lymphocytes (LYs), monocytes (MOs), eosinophils (EOs), and basophils (BAs) (left), as well as platelets (PLTs) and RBC, and the concentration of hemoglobin (Hb), in peripheral blood from *Zfp521*-CKO and *Zfp521*$^{fl/fl}$ mice. Data are from two independent experiments (A,F; mean ± SD of $n = 3$ (A) or $n = 7$ (F) mice per genotype in each) or are representative of three independent experiments (C), three independent experiments (D,E; mean ± SD of $n = 3$ mice per genotype in each). ***$p < 0.001$ (Student's t test in (D–F).

et al., 2010; Harrison et al., 1990), eventually leading to impairment of HSC pool size. We first transplanted *Zfp521*-CKO or *Zfp521*$^{fl/fl}$ BM cells into lethally irradiated wild-type recipient mice (CD45.1). Two months later, we confirmed that more than 95% of the BM cells in the recipient mice were donor-derived (Figure S2A). PB analysis revealed that *Zfp521*-CKO chimeric mice had a similar PB count compared to *Zfp521*$^{fl/fl}$ chimeric mice (Figure S2B and Table S2). The frequency of myeloid cells, B cells, T cells, and RBC in the BM of *Zfp521*-CKO chimeric mice was comparable to that of *Zfp521*$^{fl/fl}$ chimeric mice (Figures S2C and S2D). To determine whether *Zfp521* is involved in maintaining HSPC under stress *in vivo*, we characterized the compartments of HSPC in the chimeric mice by flow cytometry. We found that the absolute number and frequency of HSC and HPC were significantly lower in *Zfp521*-CKO chimeric mice compared to *Zfp521*$^{fl/fl}$ chimeric mice (Figures 3A, 3B, and 3E). Consistently, the total number of CD34$^-$LSK and LT-HSC was also significantly lower in *Zfp521*-CKO chimeric mice (Figures 3A–3C). However, the absolute number and frequency of ST-HSC and MPP were not significantly altered in *Zfp521*-CKO chimeric mice (Figures 3A and 3C).

We next characterized myeloid progenitor cells in *Zfp521*$^{fl/fl}$ and *Zfp521*-CKO chimeric mice. The frequency and total number of CMP, GMP, and MEP were significantly reduced in *Zfp521*-CKO chimeric mice compared to *Zfp521*$^{fl/fl}$ chimeric mice (Figures 3D and 3E). Lymphoid-primed MPPs (Lin$^-$Sca-1$^+$c-Kit$^+$Flk2$^+$) have the ability to differentiate into T cells, B cells, and monocytes (Adolfsson et al., 2005). *Zfp521*-CKO chimeric mice also had a lower total number and frequency of lymphoid-primed MPPs compared to the *Zfp521*$^{fl/fl}$ chimeric mice (Figures 3D and 3F).

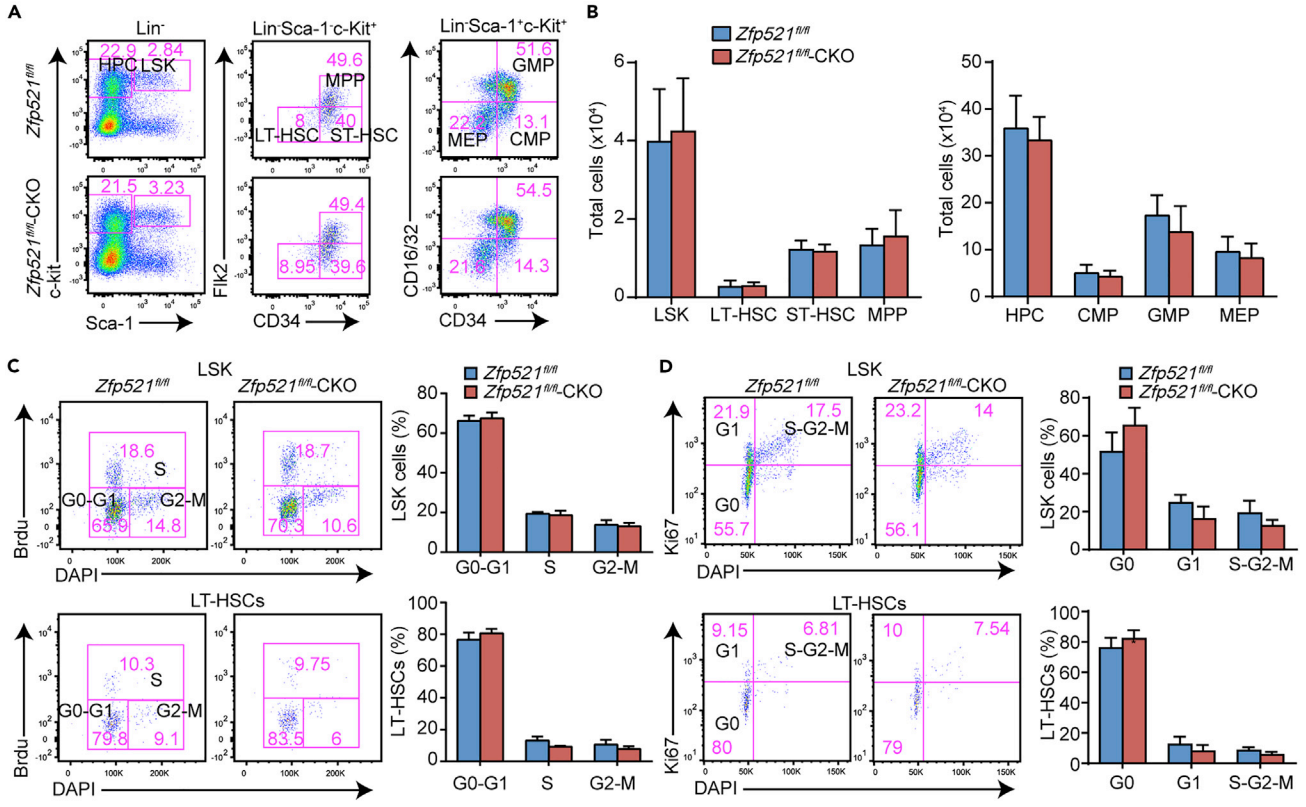

Figure 2. Depletion of *Zfp521* does not affect normal hematopoiesis

(A) Flow cytometry of BM cells from *Zfp521*$^{fl/fl}$ and *Zfp521*-CKO mice. Numbers adjacent to outlined areas indicate percent of c-Kit$^+$Sca-1$^-$ (HPC) or c-Kit$^+$Sca-1$^+$ cells (LSK cells) among Lin$^-$ cells (left panel), or CD34$^-$Flk2$^-$ cells (LT-HSC) or CD34$^+$Flk2$^-$ (ST-HSC) or CD34$^+$Flk2$^-$ (MPP) among LSK cells, or CD16/32$^-$CD34$^-$ cells (MEP) or CD16/32$^+$CD34$^+$ cells (GMP) or CD16/32$^-$CD34$^+$ cells (CMP) among HPC (right panel).

(B) Total LSK cells, LT-HSC, ST-HSC, MPP, HPC, CMP, GMP, and MEP in BM from 8- to 12-week-old *Zfp521*$^{fl/fl}$ and *Zfp521*-CKO mice.

(C) Flow cytometry analyzing the cell cycle in *Zfp521*$^{fl/fl}$ and *Zfp521*-CKO LSK cells, and LT-HSC, stained with the DNA-binding dye DAPI and labeled with bromodeoxyuridine (BrdU). Numbers adjacent to outlined areas indicate percent cells in the GO-G1 (bottom left), S (top), or G2-M (bottom right) phases of the cell cycle. Right, cell cycle profile of cells at left.

(D) Flow cytometry analyzing the cell cycle of LSK cells, and LT-HSC from *Zfp521*$^{fl/fl}$ and *Zfp521*-CKO mice. Numbers in quadrants indicate percent cells in various phases of the cell cycle: G1 (top left), S-G2-M (top right), G0 (bottom left), or other (bottom right). Right, cell cycle status of cells on the left. Data are representative of three experiments (A, C, D), or are obtained from three experiments (B and right panel of C, D; mean ± SD of n = 7–8 mice per genotype).

In addition, a colony-forming unit assay was performed to identify the frequency of myeloid progenitors in the BM cells obtained from *Zfp521*-CKO and *Zfp521*$^{fl/fl}$ chimeric mice. BM cells obtained from both genotypic chimeric mice were plated in methylcellulose medium supplemented with interleukin 3 (IL-3), interleukin 6 (IL-6), erythropoietin (EPO), and stem cell factor, and were cultured for 10–12 days. We observed that BM cells from *Zfp521*-CKO chimeric mice generated notably lower numbers of total colony-forming units, as well as colony-forming units of various myeloid precursors, including granulocyte-erythroid-macrophage-megakaryocyte colonies, granulocyte colonies, macrophage colonies, granulocyte-macrophage colonies, and burst-forming unit-erythroid colonies, than did *Zfp521*$^{fl/fl}$ chimeric BM cells (Figure 3G). As the maintenance of HSC and HPC are closely associated with cell survival, the apoptosis of LSK cells and HPC from both genotypic chimeric mice was assessed by staining cells with annexin V. We found that the frequency of apoptosis was significantly higher in LSK cells and HPC from *Zfp521*-CKO chimeric mice than that in those from *Zfp521*$^{fl/fl}$ chimeric mice at 1 month post-transplantation (Figures 3H and 3I). Meanwhile, the frequency of apoptosis remained higher in LSK and HPC cells from *Zfp521*-CKO chimeric mice at 4 month post-transplantation (Figures S3A and S3B). Similarly, the activities of caspase 3 and caspase 7 were significantly elevated in LSK cells and HSC from *Zfp521*-CKO chimeric mice (Figures 3J and 3K). Our results suggested that *Zfp521* deficiency impaired the survival of HSC and HPC under stress.

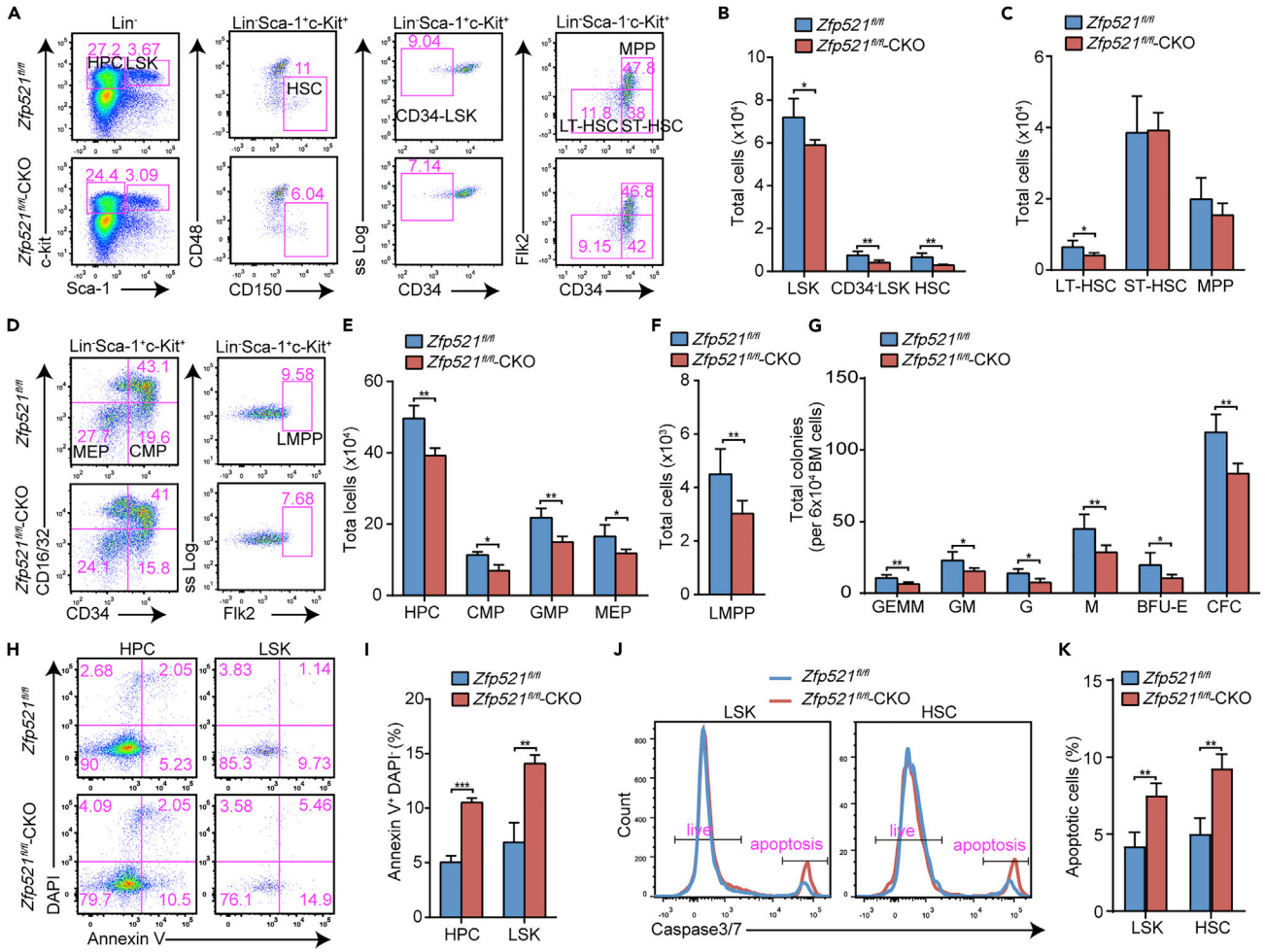

Figure 3. *Zfp521* loss impairs the size of HSC and HPC pools under stress in the chimeric mice

(A) Flow cytometry of BM cells from *Zfp521*$^{fl/fl}$ and *Zfp521*-CKO chimeric mice. Numbers adjacent to outlined areas indicate percent c-Kit$^+$Sca-1$^-$ (HPC) or c-Kit$^+$Sca-1$^+$ cells (LSK cells) among Lin$^-$ cells (far left), or CD48$^-$CD150$^+$ cells (HSC) (left), CD34$^-$ cells (right), CD34$^-$Flk2$^-$ cells (LT-HSC), CD34$^+$Flk2$^-$ (ST-HSC), or CD34$^+$Flk2$^-$ (MPP) (far right) among LSK cells. SS Log (right), side scatter log value.

(B and C) Total LSK cells, CD34$^-$LSK cells, HSC, LT-HSC, ST-HSC, and MPP in BM from 8- to 12-week-old *Zfp521*$^{fl/fl}$ and *Zfp521*-CKO chimeric mice.

(D) Flow cytometry of HPC and myeloid progenitor cells from *Zfp521*$^{fl/fl}$ and *Zfp521*-CKO chimeric mice. Numbers adjacent to outlined areas indicate percent CD16/32$^-$CD34$^-$ cells (MEP) (bottom left), CD16/32$^+$CD34$^+$ cells (GMP) (top right) or CD16/32$^-$CD34$^+$ cells (CMP) (bottom right) among HPC cells (left), or Flk2$^+$ cells (LMPP) (right) among LSK cells (right).

(E and F) Total HPC, CMP, GMP, and MEP (E) and LMPP (F) in BM from 8- to 12-week-old *Zfp521*$^{fl/fl}$ and *Zfp521*-CKO chimeric mice.

(G) *In vitro* assay of the colony-forming units of granulocyte, erythroid, macrophage, megakaryocyte colonies, granulocyte-macrophage colonies, granulocyte colonies (G), macrophage colonies (M), burst-forming unit-erythroid colonies (BFU-E), and total colony-forming cells (CFC) 10–12 d after plating of *Zfp521*$^{fl/fl}$ and *Zfp521*-CKO chimeric BM.

(H and I) Loss of *Zfp521* increases apoptosis in HPC and LSK cells. Flow cytometry images showing apoptosis in HPC and LSK cells obtained from *Zfp521*$^{fl/fl}$ and *Zfp521*-CKO chimeric mice (H). The apoptotic profile of cells are presented on (I) H.

(J and K) *Zfp521* deficiency elevates the activities of caspase 3 and caspase 7. Representative histograms for caspase 3/7 (J) and statistical results (K) are presented.

Data are representative of three experiments (A, D, H, and J) or, or are obtained from three experiments (B, C, E, F, I, and K; mean ± SD of n = 7–8 mice per genotype) or two experiments (G; mean ± SD of n = 3 mice per genotype). *p < *0.05*, **p < 0.01, ***p < 0.001 (Student's t test in B, C, E–G, I, and K).

Loss of *Zfp521* impairs the long-term self-renewal capacity of HSC

To evaluate the effects of *Zfp521* deficiency on the regenerative capacity of HSC under stress, *Zfp521*-CKO and *Zfp521*$^{fl/fl}$ chimeric mice were intraperitoneally injected with 5-fluorouracil (5-FU) weekly; this induces proliferative stress on HSC and also excludes the potential effects of 5-FU on the non-hematopoietic tissues. We observed a significantly advanced 5-FU induced hematopoietic failure in *Zfp521*-CKO chimeric

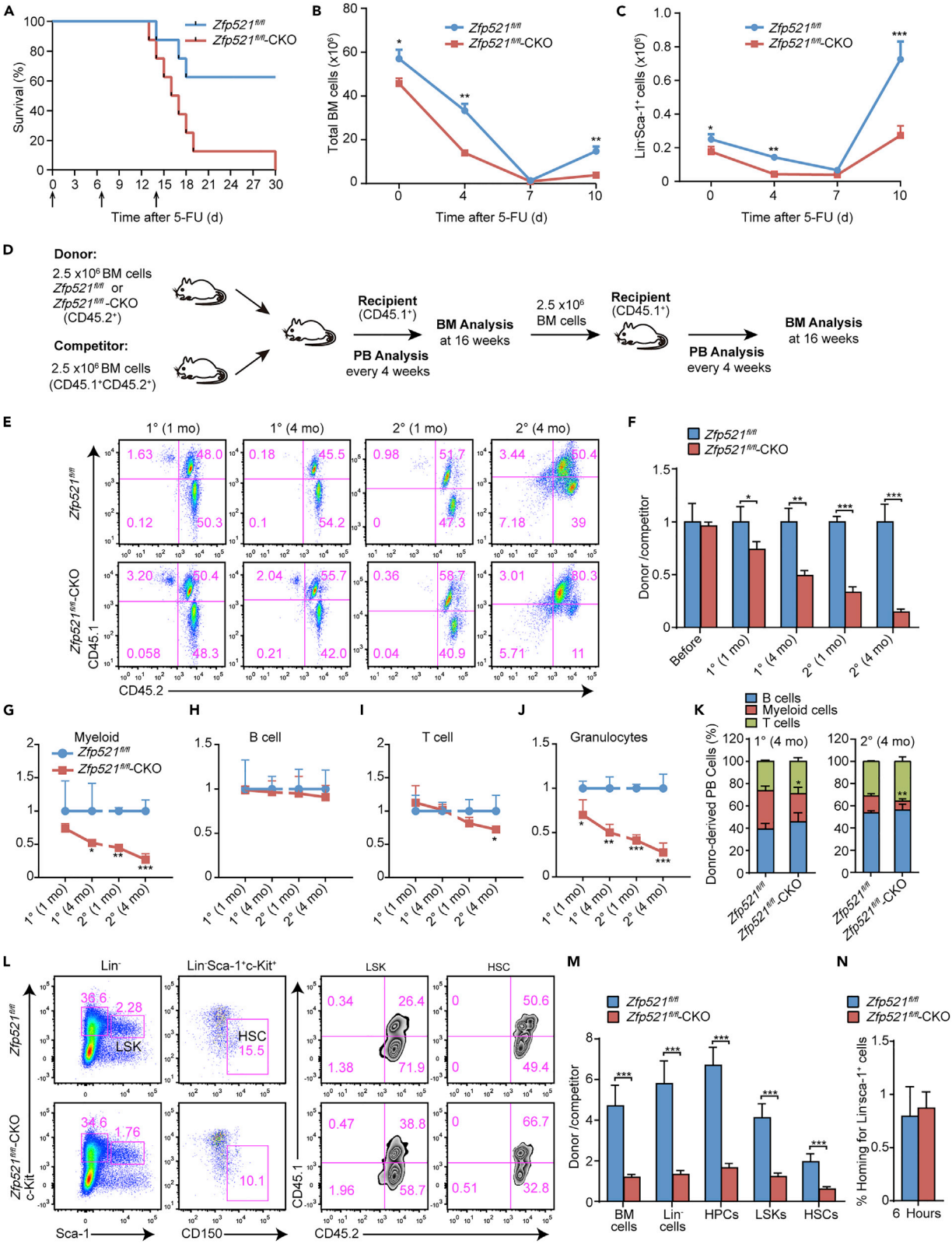
A
Survival (%)
Zfp521fl/fl
Zfp521fl/fl-CKO
Time after 5-FU (d)
B
Total BM cells (x10⁶)
Time after 5-FU (d)
C
Lin⁻Sca-1⁺ cells (x10⁶)
Time after 5-FU (d)
D
Donor:
2.5 x10⁶ BM cells
Zfp521fl/fl or
Zfp521fl/fl-CKO
(CD45.2⁺)
Competitor:
2.5 x10⁶ BM cells
(CD45.1⁺CD45.2⁺)
Recipient
(CD45.1⁺)
PB Analysis
every 4 weeks
BM Analysis
at 16 weeks
2.5 x10⁶
BM cells
Recipient
(CD45.1⁺)
PB Analysis
every 4 weeks
BM Analysis
at 16 weeks
E
1° (1 mo)
1° (4 mo)
2° (1 mo)
2° (4 mo)
Zfp521fl/fl
Zfp521fl/fl-CKO
CD45.1
CD45.2
F
Donor /competitor
Before
1° (1 mo)
1° (4 mo)
2° (1 mo)
2° (4 mo)
G
Myeloid
H
B cell
I
T cell
J
Granulocytes
K
B cells
Myeloid cells
T cells
Donro-derived PB Cells (%)
L
Lin⁻
Lin⁻Sca-1⁺c-Kit⁺
LSK
HSC
Sca-1
CD150
CD45.1
CD45.2
M
Donor /competitor
BM cells
Lin⁻ cells
HPCs
LSKs
HSCs
N
% Homing for Lin⁻sca-1⁺ cells
6 Hours

Figure 4. *Zfp521*-deficient HSC have a significantly diminished repopulation capacity in the chimeric mice

(A) Survival of *Zfp521*$^{fl/fl}$ and *Zfp521*-CKO chimeric mice after multiple injections (upward arrows) of 5-FU (50 mg per kg body weight), presented as Kaplan-Meier curves. **p < 0.01 (Mantel-Cox test).

(B and C) Total BM cells (B) and Lin$^-$Sca-1$^+$ cells (C) in *Zfp521*$^{fl/fl}$ and *Zfp521*-CKO chimeric mice before (day 0) and on days 4, 7, and 10 after injection of 5-FU.

(D) Schematic representation of serial competitive transplantation studies.

(E) Flow cytometry of peripheral blood cells from chimeric CD45.1$^+$ mice reconstituted with BM cells from *Zfp521*$^{fl/fl}$ or *Zfp521*-CKO mice, assessed at indicated time.

(F) Ratio of donor-derived CD45.2$^+$CD45.1$^-$ peripheral blood (PB) cells to competitor cell-derived CD45.1$^+$CD45.2$^+$ PB cells from mice as in E, assessed before or at 1, and 4 month after transplantation.

(G–J) The ratio of donor-derived CD45.2$^+$CD45.1$^-$ from *Zfp521*$^{fl/fl}$ or *Zfp521*-CKO vs. competitor-cell-derived CD45.1$^+$CD45.2$^+$ in myeloid cells (G), B cells (H), T cells (I), and granulocytes (J) in PB from first and secondary recipient mice were analyzed.

(K) Lineage differentiation in the mice as in E. Histogram shows percentage of donor-derived (CD45.2$^+$CD45.1$^-$) myeloid cells (Gr-1$^+$Mac$^+$), B cells (B220$^+$), and T cells (CD3$^+$) in PB analyzed 4 months after the first and secondary transplantation.

(L) Flow cytometric analysis of the frequency of LSK cells and HSC in the competitive repopulated recipient mice 4 months after secondary transplantation.

(M) Ratio of donor-derived cells to competitor cell-derived cells among total BM cells, Lin$^-$ cells, HPC, LSK cells, and HSC from recipient mice 4 months after secondary transplantation as in F.

(N) Homing ability of Lin$^-$Sca-1$^+$ hematopoietic progenitor cells from *Zfp521*$^{fl/fl}$ and *Zfp521*-CKO mice. Histograms showing the percentage of the recovered CFSE$^+$ Lin$^-$Sca-1$^+$ in the BM 6 h after transplantation.

Data are obtained from one experiment (A-C, E-L; n = 8 per genotype (A-C) or mean ± SD of n = 4–5 recipient mice per donor genotype (E-L)) or two experiments (M,N; mean ± SD of n = 5 per donor genotype). *p < 0.05, **p < 0.01, and ***p < 0.001 (Student's t test in B, C, F-K, M, N).

mice. At day 20, >80% of *Zfp521*-CKO chimeric mice died after the third injection of 5-FU, while more than 60% *Zfp521*$^{fl/fl}$ chimeric were still alive (Figure 4A). Analysis of BM cells and HSPC from another cohort of 5-FU-treated *Zfp521*-CKO and *Zfp521*$^{fl/fl}$ chimeric mice indicated that *Zfp521*-deficient HSCs failed to efficiently replenish BM cells and HSPC (Figures 4B and 4C). These data indicated that *Zfp521* deficiency decreases the recovery of HSC after 5-FU treatment.

To further assess the long-term self-renewal capacity of *Zfp521*-deficient HSC in a competitive environment, we performed competitive serial transplantation assays. An equal number of BM cells from *Zfp521*-CKO mice or their *Zfp521*$^{fl/fl}$ littermate controls (all CD45.2$^+$) were transplanted into lethally irradiated recipient mice (CD45.1$^+$) together with competitor BM cells (CD45.1$^+$CD45.2$^+$). Four months after transplantation, BM cells were obtained from the primary transplanted mice and equal numbers of those cells were transplanted into a second set of lethally irradiated mice (Figure 4D). We assessed donor-derived (CD45.2$^+$) and competitor-derived PB cells by flow cytometry every month after transplantation. Deletion of *Zfp521* led to a progressive decrease in total donor chimerism (Figures 4E and 4F). Flow cytometry analysis of the myeloid, B cell, T cell, and granulocyte lineages in PB suggested that the repopulation of B-cell lineage was not altered but the differentiation of myeloid, T cell, and granulocyte lineages was impaired significantly after the second transplantation (Figures 4G–4J), further suggestive of a deficit in HSC function following *Zfp521* loss. It is likely that depletion of *Zfp521* decreased the myeloid linage differentiation under stress (Figure 4K). In addition, we determined the relative ratio of donor-derived versus competitor-derived cells in Lin-cells, HPC, LSK cells, and HSC in BM at 4 months after the second transplantation in both *Zfp521*-CKO and *Zfp521*$^{fl/fl}$ chimeric mice. Frequencies of all subsets of primitive hematopoietic cells derived from *Zfp521*-CKO donor cells were significantly lower than that from *Zfp521*$^{fl/fl}$ donor cells (Figures 4L and 4M). These data indicate that *Zfp521*-CKO HSC have a markedly reduced reconstitution ability after serial transplantation. To rule out the possibility that the impaired self-renewal capacity of HSC was due to HSC homing defects, we evaluated the homing capacity of Lin$^-$c-Kit$^+$ CSFE$^+$ cells from *Zfp521*-CKO and *Zfp521*$^{fl/fl}$ mice, as we described previously (Hou et al., 2015). The *Zfp521*-CKO and *Zfp521*$^{fl/fl}$ BM cells had comparable homing abilities, indicating that *Zfp521* loss does not affect the homing ability of BM cells (Figure 4N). Together, these results indicated that loss of *Zfp521* impaired the long-term self-renewal capacity of HSC in a cell-intrinsic manner.

Zfp521 is required for the maintenance of HSC quiescence under stress

While it has been reported that *Zfp521* does not modulate proliferation in osteoblasts (Hesse et al., 2010), other studies have reported that perturbations of *Zfp521* expression disrupt the G1/S transition in the cell cycle (Al Dallal et al., 2016; Hiratsuka et al., 2016). To determine whether the depletion of *Zfp521* would interfere with the cell cycle in HSC, we assessed *in vivo* incorporation of the thymidine analog bromodeoxyuridine (BrdU) to investigate the cell cycle kinetics of LSK cells and HSC from *Zfp521*-CKO and *Zfp521*$^{fl/fl}$ chimeric mice.

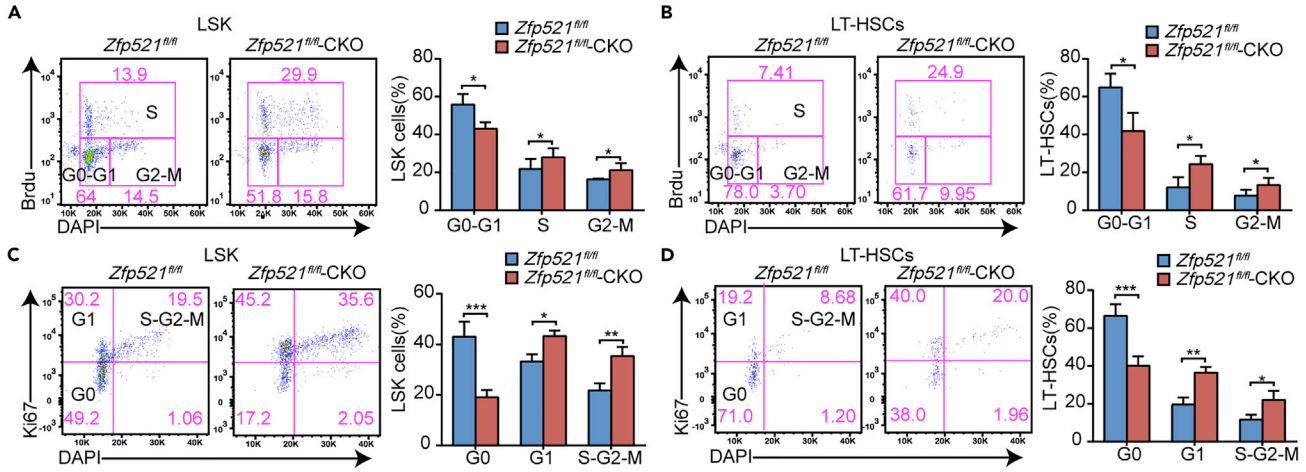

Figure 5. Deletion of *Zfp521* leads to the accumulation of cells in the S and G2-M phases of the cell cycle and loss of quiescence in HSC and LSK cells under stress in the chimeric mice

(A and B) Flow cytometry analyzing the cell cycle in LSKs (A), and LT-HSC (B) from *Zfp521*$^{fl/fl}$ and *Zfp521*-CKO chimeric mice, stained with the DNA-binding dye DAPI and labeled with BrdU. Numbers adjacent to outlined areas indicate percent cells in the GO-G1 (bottom left), S (top), or G2-M (bottom right) phases of the cell cycle. Right, cell cycle profile of cells at left.

(C and D) Flow cytometry analyzing the cell cycle of LSK (C), and LT-HSC (D) from *Zfp521*$^{fl/fl}$ and *Zfp521*-CKO chimeric mice. Numbers in quadrants indicate percent cells in various phases of the cell cycle: G1 (top left), S-G2-M (top right), G0 (bottom left), or other (bottom right). Right, cell cycle status of cells on the left. Data are representative of two experiments (mean ± SD of $n = 5$ mice per genotype). *p < 0.05, **p < 0.01, and ***p < 0.001 (Student's t test).

While ~22% of LSK cells (and ~12% of HSC) from *Zfp521*$^{fl/fl}$ were BrdU^{+}, ~30% of LSK cells (and ~20% of HSC) from *Zfp521*-CKO mice incorporated BrdU (Figures 5A and 5B). These results indicated that the absence of *Zfp521* promoted the proliferation of LSK cells and HSC. Additionally, depletion of *Zfp521* also led to the accumulation of cells at the G2-M transition phase in HSC and LSK cells (Figures 5A and 5B). Taken together, these results suggested that *Zfp521* negatively regulated the cell cycle in LSK cells and HSC in a cell context-dependent manner.

Several studies have reported that quiescence is essential for HSC to maintain their number and function (Cai et al., 2015; Hou et al., 2015; Liang et al., 2020; van Velthoven and Rando, 2019). We next investigated the fraction of LSK cells and HSC in G0 by assessing the ki67 expression and DNA content. As expected, the frequency of quiescent cells in LSK cells and HSC from *Zfp521*-CKO chimeric mice was ~1.5–2 fold lower than that in *Zfp521*$^{fl/fl}$ chimeric LSK cells and HSC (Figures 5C and 5D). This result revealed that depletion of *Zfp521* dysregulated the G0 phase in LSK cells and HSC. Thus, our data indicated that *Zfp521* was crucial for the maintenance of LSK cell and HSC quiescence under stress, and that in its deficiency, quiescent cells preferred to enter the cell cycle.

Zfp521 deficiency affects the NF-κB pathway in HSC

To further characterize *Zfp521*-dependent genes and the molecular pathways involved in the regulation of HSC function, we conducted RNA-Seq analysis of HSC sorted from *Zfp521*$^{fl/fl}$ and *Zfp521*-CKO chimeric mice 2 months after transplantation. Seventy-five differentially expressed genes were identified between *Zfp521*$^{fl/fl}$ and *Zfp521*-CKO HSC with the criteria of |log2(foldchange)|>1 and an adjusted p value of <0.05 (Figure 6A and Table S3). The differentially expressed genes were classified into seven functional groups, including genes encoding products with nucleic acid binding transcription factor activity, binding activity, catalytic activity, and structural activity (Figure 6B). Notably, upregulated genes involved in several biological processes, such as chemokine signaling pathway, positive regulation of endothelial cell proliferation, NIK/NF-κB signaling, and angiogenesis (Figure 6C), whereas downregulated genes were enriched in cell differentiation, negative regulation of NIK/NF-κB signaling, angiogenesis, and embryo development, and so on (Figure 6D). Next, we used gene set enrichment analysis to determine whether specific predefined gene sets showed significant enrichment in HSC from *Zfp521*-CKO chimeric mice by analyzing a data set that included 19,000 genes. This analysis showed enrichment for a gene set associated with NF-κB signaling in *Zfp521*-deficient HSC (Figure 6E). Notably, a gene set related with DNA replication was

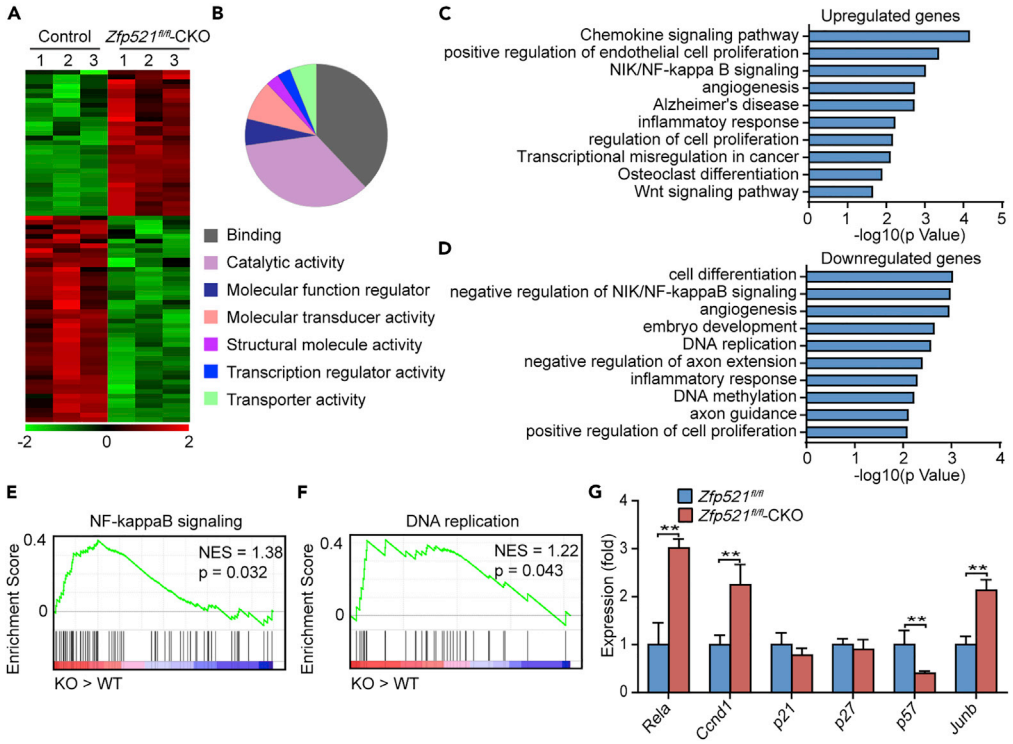

Figure 6. Genes and molecular pathways dysregulated in *Zfp521*-deficient chimeric mice HSC

(A) Heatmap of the differentially expressed genes (DEG) in HSC from *Zfp521*-CKO and *Zfp521*$^{fl/fl}$ chimeric mice.

(B) Gene ontology analysis of the DEG according to the function of their products.

(C and D) Gene ontology analysis for the upregulated (C) and downregulated (D) genes in HSC from *Zfp521*-CKO and *Zfp521*$^{fl/fl}$ chimeric mice.

(E and F) Gene set enrichment analysis of selected genes sets encoding products related to NF-κB signaling (E) and DNA replication (F), presented as enrichment score. Normalized enrichment score, 1.38, p = 0.032 (E), or 1.22, p = 0.043 (F).

(G) Quantitative real-time PCR analysis of selected genes in LT-HSC. *Actb* is used as the internal control, and the results are presented relative to those of *Zfp521*$^{fl/fl}$ control HSC. Data are from three experiments (A) or are representative of one experiment (B-F) or two experiments (G; mean ± SD). **p < 0.01 (Student's t test in G).

significantly enriched in Zpf521-deficient HSC, which was consistent with the observed increase in cycling HSC in *Zfp521*-CKO chimeric mice (Figure 6F). Thus, our results suggested that dysfunction of HSC in *Zfp521*-deficient chimeric mice were possibly associated with alteration of the NF-κB and DNA replication signaling pathway.

Rela mediates *Zfp521* function in regulating HSC quiescence

Pioneering studies have shown that constitutively active NF-κB signaling in HSC led to a decreased HSC pool, compromised HSC functions, and a hyper-proliferative phenotype associated with loss of quiescence (Nakagawa et al., 2015, 2018); this is associated with the downregulation of *Cdkn1c* (p57), and upregulation of *Ccnd1* and *Junb* (Nakagawa et al., 2015, 2018). In *Zfp521*-CKO chimeric mice, we observed a similar phenotype, and our RNA-Seq profiling data, as well as quantitative RT-PCR data, revealed that *Zfp521* deficiency in HSC was also associated with the downregulation of p57 and upregulation of *Ccnd1* and *Junb* (Figure 6G). In contrast, the expression of genes encoding p21 (*Cdkn1a*) and p27 (*Cdkn1b*) was similar in *Zfp521*$^{fl/fl}$ and *Zfp521*-CKO chimeric mice. These data implied that *Zfp521* may regulate HSC quiescence by activating the NF-κB pathway under stress.

To explore the molecular mechanisms through which *Zfp521* activates NF-κB signaling in HSC under stress, we screened the top 75 upregulated and downregulated genes in HSC from *Zfp521*-CKO mice (Figure 6A). Among these genes, the NF-κB subunit *Rela* was selected due to it displaying the most significant upregulation, with the log 2 (fold change) at 5.78, and due to its critical role in the maintenance of HSC homeostasis

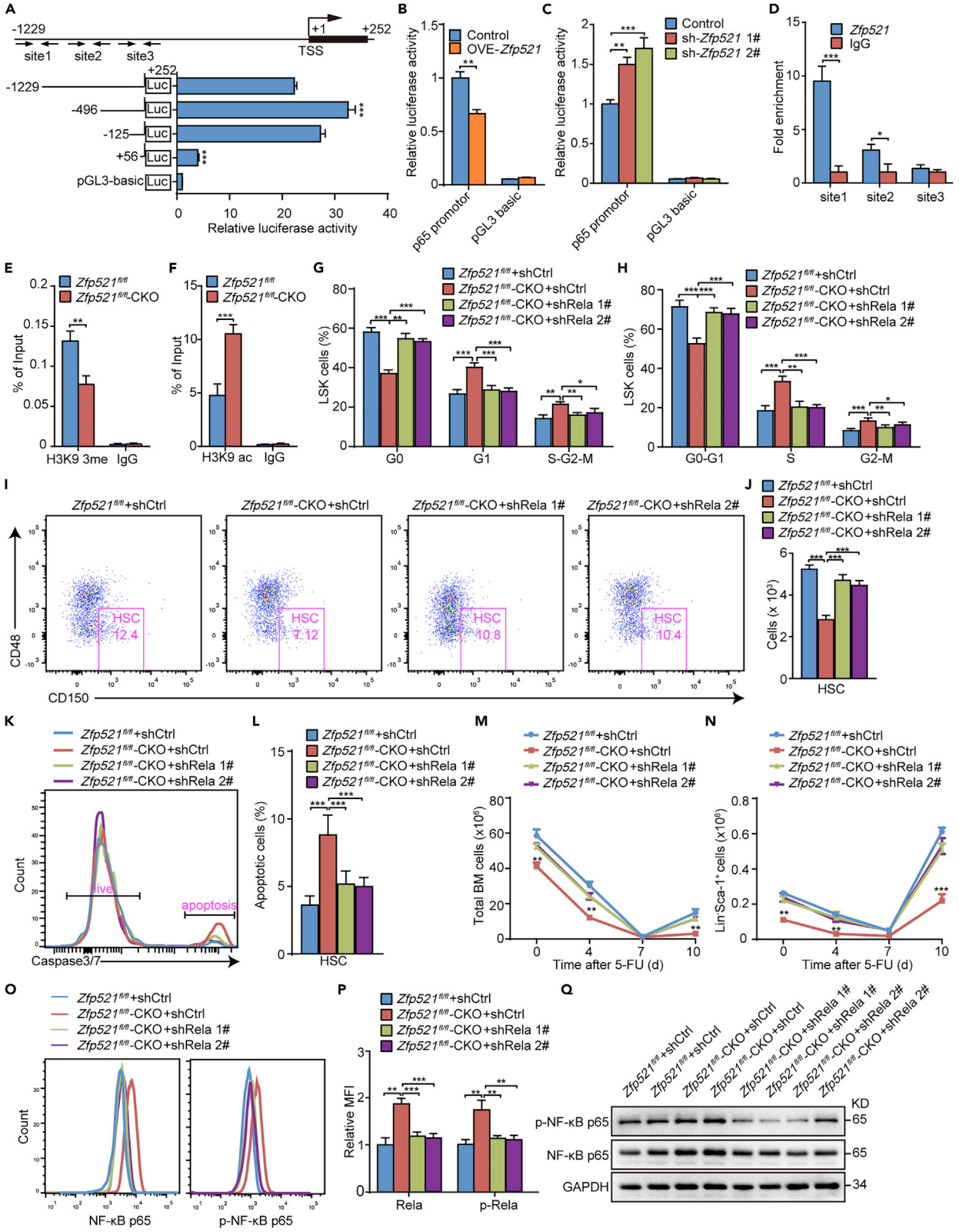
A
-1229
+1
+252
TSS
site1
site2
site3
Luc
-496
-125
+56
pGL3-basic
Relative luciferase activity
B
Control
OVE-Zfp521
Relative luciferase activity
p65 promotor
pGL3 basic
C
Control
sh-Zfp521 1#
sh-Zfp521 2#
D
Zfp521
IgG
Fold enrichment
E
Zfp521fl/fl
Zfp521fl/fl-CKO
% of Input
H3K9 3me
IgG
F
H3K9 ac
G
Zfp521fl/fl+shCtrl
Zfp521fl/fl-CKO+shCtrl
Zfp521fl/fl-CKO+shRela 1#
Zfp521fl/fl-CKO+shRela 2#
LSK cells (%)
G0
G1
S-G2-M
H
G0-G1
S
G2-M
I
CD48
CD150
HSC
J
Cells (x 10³)
K
Count
ive
apoptosis
Caspase3/7
L
Apoptotic cells (%)
M
Total BM cells (x10⁶)
Time after 5-FU (d)
N
Lin⁻Sca-1⁺ cells (x10⁶)
O
NF-κB p65
p-NF-κB p65
P
Relative MFI
Rela
p-Rela
Q
p-NF-κB p65
NF-κB p65
GAPDH
KD
65
34

Figure 7. Knockdown of *Rela* rescues *Zfp521* deficiency-induced loss of quiescence in the chimeric mice

(A) Schematic representation of *Rela* and its promoter luciferase assay. The arrows indicates primers flanking the putative ZFP521-binding sites. Luciferase assay shows the activities of a series of truncated constructs of *Rela* promoter in 293T cells.

(B and C) Luciferase activities in 293T cells transfected with the *Rela* promoter plus a vector for overexpression (B) or knockdown of *Zfp521* (C); results are presented relative to those of cells transfected with luciferase construct and empty vector.

(D) Chromatin-immunoprecipitation (ChIP) assay of the binding of endogenous *Zfp521* to the upstream region of the *Rela* promoter in 5-FU-treated BM cells from wild-type mice using primers indicated in A; IgG is used as a negative control antibody.

(E and F) ChIP assay of trimethylated histone H3 lysine 9 (H3K9me3) (E) or acetylated histone H3 lysine 9 (H3K9ac) (F) in 5-FU-treated BM cells from $Zfp521^{fl/fl}$ or *Zfp521*-CKO chimeric mice. IgG serves as a negative control.

(G) Summary of cell cycle status in LSK cells from lethally irradiated recipient mice reconstituted with $Zfp521^{fl/fl}$ or *Zfp521*-CKO BM cells transduced with control vector or shRNA against *Rela*.

(H) Summary of frequency of $BrdU^+$ LSK cells as described in G.

(I) Flow cytometry of BM cells from mice as described in G (numbers indicated frequency of HSC).

(J) Total number of HSC from mice as in G.

(K and L) The activities of caspase 3 and caspase 7 in HSC from mice as described in G. Representative histograms for caspase 3/7 (K) and statistical results (L) are presented.

(M and N) Total numbers of BM cells (M) and $Lin^-Sca\text{-}1^+$ cells (N) in another cohort of mice as described in G before (day 0) and on days 4, 7 and 10 after injection of 5-FU.

(O and P) Representative fluorescence-activated cell sorting plot (O) and quantification of the expression of NF-κB p65 and phosphorylated NF-κB p65 measured by indicated antibodies in LSK cells from mice as described in G (P).

(Q) Western blot analysis of the expression of NF-κB p65 and phosphorylated NF-κB p65 in Lin^- BM cells from mice as described in G. GAPDH was used as an internal control.

Data are from three experiments (mean ± SD of $n = 3$ (A-F), $n = 5$ mice per genotype (G, H, J, P)), or one experiments (mean ± SD of $n = 5$ (L), $n = 3$ mice per genotype (M, N)), or are representative of one experiments (K) or three experiments (I, O, Q). *$p < 0.05$, **$p < 0.01$, and ***$p < 0.001$ (One way analysis of variance [ANOVA] with Bonferroni post-tests in A, J, L, two-way ANOVA in C, G, H, M, N, P, Student's t test in B, D-F).

(Stein and Baldwin, 2013). We hypothesized that *Zfp521* deficiency activates the NF-κB pathway by upregulating *Rela*, and further regulate the quiescence of HSC.

Given the upregulation of *Rela* in *Zfp521*-deficient HSCs, we intended to investigate whether *Zfp521* can negatively regulated the expression of *Rela in vitro*. Knockdown of *ZNF521* (the homolog of *Zfp521* in humans) in 293T cells led to a striking upregulation of *RELA* expression, while, overexpression of *ZNF521* inhibited the expression of *RELA* (Figures S4A and S4B). These results suggested that *Zfp521* may act as a negative regulator of *Rela*. To explore whether *Zfp521* regulates *Rela* expression through direct transcriptional repression, we performed dual-luciferase reporter assays with cells expressing the putative promoter of mouse *Rela*. The luciferase activity of the putative mouse *Rela* promoter was inhibited by *Zfp521* overexpression, while it was activated by knockdown of *Zfp521* (Figures 7A–7C). These results suggested that *Zfp521* inhibited the expression of *Rela* through direct transcriptional repression of *Rela* by binding to its promoter. The luciferase activity of *Rela* promoter −1229 to +252 was significantly lower than that of promoter −496 to +252, thus we inferred that there are *Zfp521* binding sites between −1229 to −496. To validate our hypothesis, we performed a chromatin-immunoprecipitation (ChIP) assay of BM cells harvested from 5-FU-treated mice. Our data showed that *Zfp521* directly binds to the promoter of *Rela* (Figure 7D), which is consistent with the dual-luciferase reporter assays. Moreover, to investigate whether *Zfp521* associated with the *Rela* promoter is related to transcriptional silencing, we performed ChIP assays of BM cells from 5-FU-treated mice using histone H3K9 acetylation and H3K9 trimethylation antibodies, which are epigenetic markers of transcriptionally active and silent chromatin, respectively. We observed an increased H3K9 acetylation and decreased H3K9me3 in the promoter region of *Rela* in *Zfp521*-deficient BM cells (Figures 7E and 7F). Taken together, our data indicated that *Zfp521* directly binds to regulatory regions of the *Rela* promoter and repressed its transcription by facilitating transcriptional silencing of the *Rela* locus.

To determine whether the loss of quiescence observed in *Zfp521*-deficient LSK cells was mainly caused by upregulation of *Rela*, we investigated the effect of knockdown of *Rela* on the quiescence of *Zfp521*-deficient LSK cells *in vivo*. BM cells obtained from $Zfp521^{fl/fl}$ and *Zfp521*-CKO mice were infected with control lentivirus or lentivirus carrying shRNAs against *Rela*, and these cells were transplanted into lethally irradiated recipient mice to generate chimeric mice. BM cells were collected from chimeric mice at 6 weeks after transplantation and analyzed by flow cytometry. Notably, the frequencies of quiescent cells and $BrdU^+$ cells were significantly higher in *Rela*-specific shRNA-transduced *Zfp521*-CKO LSK cells than that in control vector-transduced *Zfp521*-CKO LSK cells in chimeric mice (Figures 7G and 7H). In addition, the frequency of LT-HSC was higher in BM cells from *Rela*-specific shRNA-transduced *Zfp521*-CKO chimeric mice than that in control vector-transduced *Zfp521*-CKO chimeric mice (Figures 7I and 7J). The activities of Caspase

3 and Caspase 7 was decreased in HSCs from *Rela*-specific shRNA-transduced *Zfp521*-CKO chimeric mice comparing with that in control vector-transduced *Zfp521*-CKO chimeric mice (Figures 7K and 7L). Furthermore, the capability of hematopoietic reconstitution of BM cells and HSPCs was better in 5-FU-treated *Rela*-specific shRNA-transduced *Zfp521*-CKO chimeric mice than that in control vector-transduced *Zfp521*-CKO chimeric mice (Figures 7M and 7N). Meanwhile, the expression level of NF-κB and phosphorylated NF-κB was higher in control vector-transduced *Zfp521*-CKO LSK cells than that in control vector-transduced $Zfp521^{fl/fl}$ or *Rela*-specific shRNA-transduced *Zfp521*-CKO LSK cells (Figures 7O–7Q). These results indicated that knockdown of *Rela* rescued the hyper-activated NF-κB pathway and prevented the depletion of LSK cells and LT-HSC induced by the *Zfp521* deficiency. In conclusion, these data suggested that *Rela* mediated or at least partly mediated *Zfp521* deficiency-induced depletion of quiescence in LSK cells by regulating the NF-κB pathway.

DISCUSSION

The role of endogenous *Zfp521* in adult hematopoiesis has not been reported. In this study, we have identified a previously unrecognized role for *Zfp521* in the maintenance of HSC and HPC in adult hematopoiesis. Using conditional deletion mouse models of *Zfp521*, we have determined that *Zfp521* was essential for the maintenance of the quiescence and self-renewal capacity of HSC *in vivo*, and that it intrinsically regulated the proliferation of HSC and HPC. We have further identified *Zfp521* as an upstream regulator of NF-κB signaling by transcriptional regulation of *Rela*, which was able to mediate the function of *Zfp521* in regulating HSC quiescence.

Zfp521 has been consistently reported as a key regulator of HSC self-renewal and differentiation in embryonic hematopoiesis (Fleenor et al., 2018; Garrison et al., 2017). However, to the best of our knowledge, the *in vivo* role of *Zfp521* in adult HSC has not yet been characterized. In our study, conditional deletion of *Zfp521* in hematopoietic compartments was efficiently induced in adult mice by intraperitoneal injection of poly(I:C). We found that the primary *Zfp521*-CKO mice had a normal frequency of mature blood cells and HSPCs, indicating that *Zfp521* is dispensable in adult HSC under homeostatic conditions. However, *Zfp521* deficiency decreased the size of the HSC pool and exhibited a diminished long-term repopulating activity in response to regenerative stress, which is consistent with previously reports in a competitive serial transplantation assay with fetal liver cells (Garrison et al., 2017). Quiescence are critical for the maintenance of HSC (van Velthoven and Rando, 2019). We first revealed that *Zfp521* depletion does not affect quiescence of HSC and LSK cells in the homeostatic state, but it significantly reduces quiescence and survival of those cell populations under stress. The decrease in quiescence and survival leads to the impaired self-renewal capacity of *Zfp521*-deficient HSC under stress conditions. All of the data we collected from the *Zfp521*-CKO chimeric mice demonstrated that *Zfp521* regulated the HSC quiescence and self-renewal in an HSC-intrinsic manner. After analyze the $Zfp521^{-/-}$ and littermate control mice at 3 weeks of age, Fleenor CJ, et al. found that $Zfp521^{-/-}$ mice possess decreased frequencies and numbers of HSPC, which is due to the fact that *Zfp521* deficiency changes BM microenvironment cytokine levels and gene expression within resident HSPC (Fleenor et al., 2018). Their data revealed that *Zfp521* regulates HSC through cell-extrinsic mechanisms in the BM microenvironment. Together, these results indicate that *Zfp521* regulates the quiescence and self-renewal of HSC in both intrinsic and extrinsic manners. Furthermore, it might make sense that the phenotypes of $Zfp521^{-/-}$ are more obvious than that in *Zfp521*-CKO mice, it is likely due to the critical role of *Zfp521* in regulation of adipocytes, osteoblasts, and osteoclasts in the BM microenvironment (Addison et al., 2014; Hesse et al., 2010; Kang et al., 2012a; Wu et al., 2009). *Zfp521* depletion elevates T cell reconstitution at 8 and 12 weeks after transplantation *in vivo* (Garrison et al., 2017) and increases B-cell differentiation *in vitro* (Al Dallal et al., 2016). However, we only observed a slight increase in T cell frequency at 4 weeks after primary transplantation, and then a moderate decrease at 16 weeks after secondary transplantation. We also found that transplantation of *Zfp521*-deficient donor cells did not increase B-cell reconstitution, which is similar to the results of a previous study (Garrison et al., 2017).

Notably, long-term exposure of HSC to proinflammatory cytokines cause diminished self-renewal and quiescence (Baldridge et al., 2010; Essers et al., 2009; Sato et al., 2009). Indeed, deregulated NF-κB activity leads to increased expression of proinflammatory cytokines, including TNF, IL1, IL6, and IFN-γ (Boone et al., 2004; Coornaert et al., 2009; Dong et al., 2010; Harhaj and Dixit, 2012). Defects in the negative regulatory circuits of NF-κB signaling cause a loss of quiescence and pre-mature depletion of HSC (Nakagawa et al., 2015). Similarly, constitutive activation of NF-κB leads to a reduced HSC pool and compromised HSC functions (Nakagawa et al., 2018). These studies highlight the critical role of NF-κB signaling in HSC

quiescence. In our study, *Zfp521* deficiency led to the upregulation of *Rela* and *Junb*, the key effector of the NF-κB pathway and its downstream target gene, respectively, and downregulation of p57, whose genes encode cyclin-dependent kinase inhibitors. Notably, constitutive activation of the NF-κB pathway obviously impairs the quiescence of HSC and their capacity for self-renewal, and is associated with upregulation of *Junb* and downregulation of the p57 genes in HSC (Nakagawa et al., 2018). *Zfp521* has revealed a vital role in epigenetic regulation of the transcription of its target genes by binding to chromatin and promoting chromatin remolding via its N-terminal NuRD motif, which binds to nucleosome remodeling and deacetylase corepressor complex (Addison et al., 2014; Al Dallal et al., 2016; Behrouznezhad et al., 2019; Yamasaki et al., 2010). Finally, our studies indicated that *Zfp521* depletion promoted *Rela* expression by directly binding its promoter, which increased H3K9 acetylation and decreased H3K9me3 in the *Rela* promoter region, indicating an increase in the transcriptional activity of *Rela*. Meanwhile, shRNA-mediated knockdown of *Rela* reversed the loss of quiescence in *Zfp521*-deficient HSPC. Taken together, these results suggest that *Zfp521* regulates HSC quiescence through control of *Rela*-mediated NF-κB signaling. Nevertheless, analysis of global gene expression in *Zfp521*-deficient and *Zfp521*-sufficient LT-HSC suggested that *Zfp521* regulates the function of HSC through multiple molecular pathways. Further detailed research is needed to investigate whether other pathways are critical for mediating *Zfp521* function in HSC.

We found that depletion of *Zfp521* increased apoptosis in HPC and LSK cells under stress, which reflects the previously observed pro-survival activity of *Zfp521* (Al Dallal et al., 2016; Correa et al., 2010; Seriwatanachai et al., 2011). Loss of *Zfp521* increases Caspase-3 activation and decreases the expression of the key apoptosis inhibitor BCL-2 (Correa et al., 2010; Yamasaki et al., 2010), which is likely to be the reason for increased apoptosis in HPC and LSK cells in *Zfp521*-deficient mice. In summary, we have provided functional and molecular evidence that *Zfp521* acts as a critical regulator of the quiescence and self-renewal of adult HSC in a cell-intrinsic manner, and *Zfp521* may regulate HSC quiescence by activating the NF-κB pathway under stress.

Limitations of the study

This study demonstrated that *Zfp521* was essential for the maintenance of the quiescence and self-renewal capacity of adult HSC under stress. Although we proposed that *Zfp521* regulates the expression of Rela by binding to its promoter region, we could not specify the detailed binding site.

Resource availability

Lead contact

Further information and requests for resources and reagents should be directed to and will be fulfilled by the lead contact, Yu Hou (houyuxn@vip.126.com).

Materials availability

Materials generated in this study will be made available upon reasonable request and may require a material transfer agreement.

Data and code availability

The RNA-seq data generated during this study are available at GEO (GSE163684).

METHODS

All methods can be found in the accompanying Transparent Methods supplemental file.

SUPPLEMENTAL INFORMATION

Supplemental Information can be found online at https://doi.org/10.1016/j.isci.2021.102039.

ACKNOWLEDGMENTS

This work was supported by grants National Key R&D Program of China (2017YFA0106700), National Natural Science Foundation of China (81670096), Army Major Scientific Research Projects (AWS17J007), and Military Emphasis Medical Scientific Research Project Fund (BWS13C018).

AUTHOR CONTRIBUTIONS

Conceptualization, J.C. and Y.H.; Methodology, Z.L.; Formal Analysis, Z.L., X.F., and Y.H.; Investigation, Z.L., X.F., W.W., Z.L.L., Z.C., C.Z., Y.L., M.K., F.S., F.X., Y.X.H., X.Z., S.F., G.Z., and X.H.; Writing - Original Draft, Z.L.; Writing -Review & Editing, Z.L. and Y.H.; Supervision, J.C. and Y.H.; Project Administration, J.C. and Y.H.

DECLARATION OF INTERESTS

The authors declare no competing interest.

Received: September 4, 2020
Revised: November 29, 2020
Accepted: January 4, 2021
Published: February 19, 2021

REFERENCES

Addison, W.N., Fu, M.M., Yang, H.X., Lin, Z., Nagano, K., Gori, F., and Baron, R. (2014). Direct transcriptional repression of Zfp423 by Zfp521 mediates a bone morphogenic protein-dependent osteoblast versus adipocyte lineage commitment switch. Mol. Cell. Biol. *34*, 3076–3085.

Adolfsson, J., Mansson, R., Buza-Vidas, N., Hultquist, A., Liuba, K., Jensen, C.T., Bryder, D., Yang, L., Borge, O.J., Thoren, L.A., et al. (2005). Identification of Flt3+ lympho-myeloid stem cells lacking erythro-megakaryocytic potential a revised road map for adult blood lineage commitment. Cell *121*, 295–306.

Al Dallal, S., Wolton, K., and Hentges, K.E. (2016). Zfp521 promotes B-cell viability and cyclin D1 gene expression in a B cell culture system. Leuk. Res. *46*, 10–17.

Baldridge, M.T., King, K.Y., Boles, N.C., Weksberg, D.C., and Goodell, M.A. (2010). Quiescent haematopoietic stem cells are activated by IFN-gamma in response to chronic infection. Nature *465*, 793–797.

Behrouznezhad, F., Ejeian, F., Emadi-Baygi, M., Nikpour, P., and Nasr-Esfahani, M.H. (2019). Hypothesis: a challenge of overexpression Zfp521 in neural tendency of derived dental pulp stem cells. Cell J. *21*, 99–102.

Bond, H.M., Mesuraca, M., Carbone, E., Bonelli, P., Agosti, V., Amodio, N., De Rosa, G., Di Nicola, M., Gianni, A.M., Moore, M.A., et al. (2004). Early hematopoietic zinc finger protein (EHZF), the human homolog to mouse Evi3, is highly expressed in primitive human hematopoietic cells. Blood *103*, 2062–2070.

Boone, D.L., Turer, E.E., Lee, E.G., Ahmad, R.C., Wheeler, M.T., Tsui, C., Hurley, P., Chien, M., Chai, S., Hitotsumatsu, O., et al. (2004). The ubiquitin-modifying enzyme A20 is required for termination of Toll-like receptor responses. Nat. Immunol. *5*, 1052–1060.

Cai, X., Gao, L., Teng, L., Ge, J., Oo, Z.M., Kumar, A.R., Gilliland, D.G., Mason, P.J., Tan, K., and Speck, N.A. (2015). Runx1 deficiency decreases ribosome biogenesis and confers stress resistance to hematopoietic stem and progenitor cells. Cell Stem Cell *17*, 165–177.

Cheshier, S.H., Morrison, S.J., Liao, X., and Weissman, I.L. (1999). In vivo proliferation and cell cycle kinetics of long-term self-renewing hematopoietic stem cells. Proc. Natl. Acad. Sci. U S A *96*, 3120–3125.

Coornaert, B., Carpentier, I., and Beyaert, R. (2009). A20: central gatekeeper in inflammation and immunity. J. Biol. Chem. *284*, 8217–8221.

Correa, D., Hesse, E., Seriwatanachai, D., Kiviranta, R., Saito, H., Yamana, K., Neff, L., Atfi, A., Coillard, L., Sitara, D., et al. (2010). Zfp521 is a target gene and key effector of parathyroid hormone-related peptide signaling in growth plate chondrocytes. Dev. Cell *19*, 533–546.

Dong, J., Jimi, E., Zeiss, C., Hayden, M.S., and Ghosh, S. (2010). Constitutively active NF-kappaB triggers systemic TNFalpha-dependent inflammation and localized TNFalpha-independent inflammatory disease. Genes Dev. *24*, 1709–1717.

Dzierzak, E., and Speck, N. (2008). Of lineage and legacy: the development of mammalian hematopoietic stem cells. Nature Immunol. *9*, 129–136.

Enver, T., Heyworth, C.M., and Dexter, T.M. (1998). Do stem cells play dice? Blood *92*, 348–351, discussion 352.

Essers, M.A., Offner, S., Blanco-Bose, W.E., Waibler, Z., Kalinke, U., Duchosal, M.A., and Trumpp, A. (2009). IFNalpha activates dormant haematopoietic stem cells in vivo. Nature *458*, 904–908.

Fleenor, C.J., Arends, T., Lei, H., Ahsberg, J., Okuyama, K., Kuruvilla, J., Cristobal, S., Rabe, J.L., Pandey, A., Danhorn, T., et al. (2018). Zinc finger protein 521 regulates early hematopoiesis through cell-extrinsic mechanisms in the bone marrow microenvironment. Mol. Cell. Biol. *38*, e00603-17.

Garrison, B.S., Rybak, A.P., Beerman, I., Heesters, B., Mercier, F.E., Scadden, D.T., Bryder, D., Baron, R., and Rossi, D.J. (2017). ZFP521 regulates murine hematopoietic stem cell function and facilitates MLL-AF9 leukemogenesis in mouse and human cells. Blood *130*, 619–624.

Harhaj, E.W., and Dixit, V.M. (2012). Regulation of NF-kappaB by deubiquitinases. Immunol. Rev. *246*, 107–124.

Harrison, D.E., Stone, M., and Astle, C.M. (1990). Effects of transplantation on the primitive immunohematopoietic stem cell. J. Exp. Med. *172*, 431–437.

Hesse, E., Saito, H., Kiviranta, R., Correa, D., Yamana, K., Neff, L., Toben, D., Duda, G., Atfi, A., Geoffroy, V., et al. (2010). Zfp521 controls bone mass by HDAC3-dependent attenuation of Runx2 activity. J. Cell Biol. *191*, 1271–1283.

Hiratsuka, T., Takei, Y., Ohmori, R., Imai, Y., Ozeki, M., Tamaki, K., Haga, H., Nakamura, T., and Tsuruyama, T. (2016). ZFP521 contributes to pre-B-cell lymphomagenesis through modulation of the pre-B-cell receptor signaling pathway. Oncogene *35*, 3227–3238.

Hou, Y., Li, W., Sheng, Y., Li, L., Huang, Y., Zhang, Z., Zhu, T., Peace, D., Quigley, J.G., Wu, W., et al. (2015). The transcription factor Foxm1 is essential for the quiescence and maintenance of hematopoietic stem cells. Nat. Immunol. *16*, 810–818.

Kamiya, D., Banno, S., Sasai, N., Ohgushi, M., Inomata, H., Watanabe, K., Kawada, M., Yakura, R., Kiyonari, H., Nakao, K., et al. (2011). Intrinsic transition of embryonic stem-cell differentiation into neural progenitors. Nature *470*, 503–509.

Kang, S., Akerblad, P., Kiviranta, R., Gupta, R.K., Kajimura, S., Griffin, M.J., Min, J., Baron, R., and Rosen, E.D. (2012a). Regulation of early adipose commitment by Zfp521. PLoS Biol. *10*, e1001433.

Kang, S., Akerblad, P., Kiviranta, R., Gupta, R.K., Kajimura, S., Griffin, M.J., Min, J., Baron, R., and Rosen, E.D. (2012b). Regulation of early adipose commitment by Zfp521. PLoS Biol. *10*, e1001433.

Kiviranta, R., Yamana, K., Saito, H., Ho, D.K., Laine, J., Tarkkonen, K., Nieminen-Pihala, V., Hesse, E., Correa, D., Maatta, J., et al. (2013). Coordinated transcriptional regulation of bone homeostasis by Ebf1 and Zfp521 in both mesenchymal and hematopoietic lineages. J. Exp. Med. *210*, 969–985.

Liang, R., Arif, T., Kalmykova, S., Kasianov, A., Lin, M., Menon, V., Qiu, J., Bernitz, J.M., Moore, K., Lin, F., et al. (2020). Restraining lysosomal activity

preserves hematopoietic stem cell quiescence and potency. Cell Stem Cell *26*, 359–376.e7.

Lin, A.C., Roche, A.E., Wilk, J., and Svensson, E.C. (2004). The N termini of Friend of GATA (FOG) proteins define a novel transcriptional repression motif and a superfamily of transcriptional repressors. J. Biol. Chem. *279*, 55017–55023.

Matsubara, E., Sakai, I., Yamanouchi, J., Fujiwara, H., Yakushijin, Y., Hato, T., Shigemoto, K., and Yasukawa, M. (2009). The role of zinc finger protein 521/early hematopoietic zinc finger protein in erythroid cell differentiation. J. Biol. Chem. *284*, 3480–3487.

Mega, T., Lupia, M., Amodio, N., Horton, S.J., Mesuraca, M., Pelaggi, D., Agosti, V., Grieco, M., Chiarella, E., Spina, R., et al. (2011). Zinc finger protein 521 antagonizes early B-cell factor 1 and modulates the B-lymphoid differentiation of primary hematopoietic progenitors. Cell Cycle *10*, 2129–2139.

Nakagawa, M.M., Chen, H., and Rathinam, C.V. (2018). Constitutive activation of NF-kappaB pathway in hematopoietic stem cells causes loss of quiescence and deregulated transcription factor networks. Front. Cell Dev. Biol. *6*, 143.

Nakagawa, M.M., Thummar, K., Mandelbaum, J., Pasqualucci, L., and Rathinam, C.V. (2015). Lack of the ubiquitin-editing enzyme A20 results in loss of hematopoietic stem cell quiescence. J. Exp. Med. *212*, 203–216.

Sato, T., Onai, N., Yoshihara, H., Arai, F., Suda, T., and Ohteki, T. (2009). Interferon regulatory factor-2 protects quiescent hematopoietic stem cells from type I interferon-dependent exhaustion. Nat. Med. *15*, 696–700.

Seriwatanachai, D., Densmore, M.J., Sato, T., Correa, D., Neff, L., Baron, R., and Lanske, B. (2011). Deletion of Zfp521 rescues the growth plate phenotype in a mouse model of Jansen metaphyseal chondrodysplasia. FASEB J. *25*, 3057–3067.

Shahbazi, E., Moradi, S., Nemati, S., Satarian, L., Basiri, M., Gourabi, H., Zare Mehrjardi, N., Gunther, P., Lampert, A., Handler, K., et al. (2016). Conversion of human fibroblasts to stably self-renewing neural stem cells with a single zinc-finger transcription factor. Stem Cell Reports *6*, 539–551.

Stein, S.J., and Baldwin, A.S. (2013). Deletion of the NF-kappaB subunit p65/RelA in the hematopoietic compartment leads to defects in hematopoietic stem cell function. Blood *121*, 5015–5024.

van Velthoven, C.T.J., and Rando, T.A. (2019). Stem cell quiescence: dynamism, restraint, and cellular idling. Cell Stem Cell *24*, 213–225.

Wilkinson, A.C., Igarashi, K.J., and Nakauchi, H. (2020). Haematopoietic stem cell self-renewal in vivo and ex vivo. Nat. Rev. Genet. *21*, 541–554.

Wu, M., Hesse, E., Morvan, F., Zhang, J.P., Correa, D., Rowe, G.C., Kiviranta, R., Neff, L., Philbrick, W.M., Horne, W.C., et al. (2009). Zfp521 antagonizes Runx2, delays osteoblast differentiation in vitro, and promotes bone formation in vivo. Bone *44*, 528–536.

Yamasaki, N., Miyazaki, K., Nagamachi, A., Koller, R., Oda, H., Miyazaki, M., Sasaki, T., Honda, Z.I., Wolff, L., Inaba, T., et al. (2010). Identification of Zfp521/ZNF521 as a cooperative gene for E2A-HLF to develop acute B-lineage leukemia. Oncogene *29*, 1963–1975.

iScience, Volume *24*

Supplemental Information

Zfp521 is essential for the quiescence and maintenance of adult hematopoietic stem cells under stress

Zhigang Li, Xuemei Fu, Weiru Wu, Zhilong Liu, Zhe Chen, Chengfang Zhou, Yuanyuan Liu, Mei Kuang, Fangfang Sun, Feifei Xiao, Yongxiu Huang, Xiaojun Zhang, Shijun Fan, Xingqin Huang, Guangling Zheng, Jieping Chen, and Yu Hou

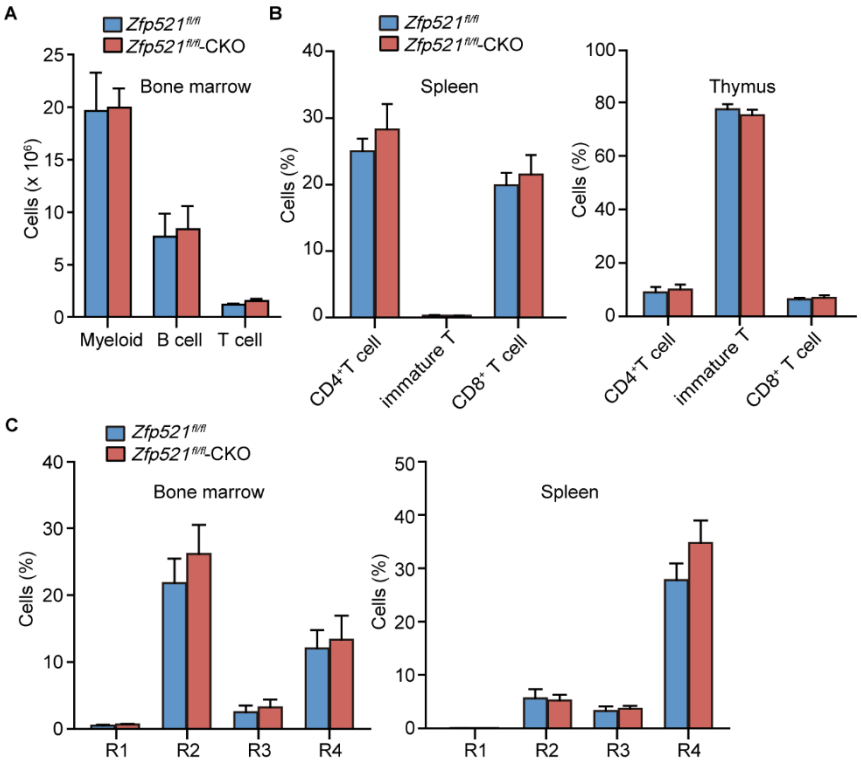

Figure S1. Depletion of *Zfp521* does not affect the frequency of mature blood cells. Related to Figure 1.

(**A**) Histograms represent the frequency of myeloid cells (Mac-1$^+$ Gr$^+$), B cells (B220$^+$ IgM$^+$), and T cells (CD4$^+$CD8$^+$) in BM from *Zfp521*$^{fl/fl}$-CKO and *Zfp521*$^{fl/fl}$ mice. (**B**) Histograms represent the frequency of three differentiation stages of T cells including CD4$^+$CD8$^-$, CD4$^+$CD8$^+$, and CD4$^-$CD8$^+$ in spleen cells (left panel) and thymus cells (right panel) from *Zfp521*$^{fl/fl}$ -CKO and *Zfp521*$^{fl/fl}$ mice. (**C**) The frequency and representative flow cytometric histograms of four differentiation stages of erythroblasts including R1 (CD71$^+$Ter119$^-$), R2 (CD71$^+$Ter119$^+$), R3 (CD71^{low}Ter119$^+$), and R4 (CD71$^-$Ter119$^+$) in BM cells (left panel) and spleen cells (right panel) from *Zfp521*$^{fl/fl}$ -CKO and *Zfp521*$^{fl/fl}$ mice. Data are from three independent experiments (mean ± SD of *n* = 5 mice per genotype in each).

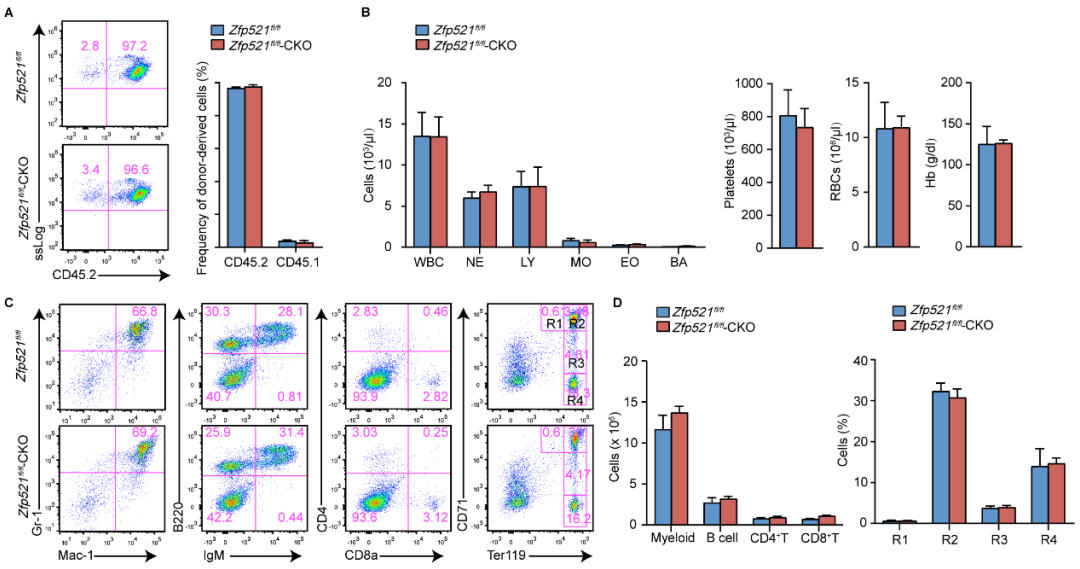

Figure S2. *Zfp521* loss does not interfere with the number of mature blood cells and lineage differentiation under stress. Related to Figure 3.

(**A**) Flow cytometric analysis of the frequency of donor-derived BM cells in *Zfp521*-CKO and *Zfp521*$^{fl/fl}$ chimeric mice. (**B**) Absolute number of white blood cells (WBC), neutrophils (NE), lymphocytes (LY), monocytes (MO), eosinophils (EO), and basophils (BA) (left), as well as platelets (PLT) and red blood cells (RBC), and the concentration of hemoglobin (Hb), in the peripheral blood from *Zfp521*-CKO and *Zfp521*$^{fl/fl}$ chimeric mice. (**C**) Representative diagrams show the frequency of myeloid cells (Mac-1$^+$ Gr$^+$), B cells (B220$^+$ IgM$^+$), T cells (CD4$^+$CD8$^+$), and red blood cells (CD71$^+$Ter119$^+$) in BM from *Zfp521*$^{fl/fl}$-CKO and *Zfp521*$^{fl/fl}$ chimeric mice. (**D**) Histograms represent the total number of myeloid cells (Mac-1$^+$ Gr-1$^+$), B cells (B220$^+$ IgM$^+$), CD4$^+$ T cells, CD8$^+$ T cells (left panel), and frequency of four differentiation stages of erythroblasts including R1 (CD71$^+$Ter119$^-$), R2 (CD71$^+$Ter119$^+$), R3 (CD71^{low}Ter119$^+$), and R4 (CD71$^-$Ter119$^+$) in BM cells from *Zfp521*$^{fl/fl}$ -CKO and *Zfp521*$^{fl/fl}$ mice. Data are from two independent experiments (**B**; mean ± SD of *n* = 7 mice per genotype) or three independent experiments (**right panel in A**, **D**; mean ± SD of *n* = 5 mice per genotype) or are representative of three experiments (**A**, **C**).

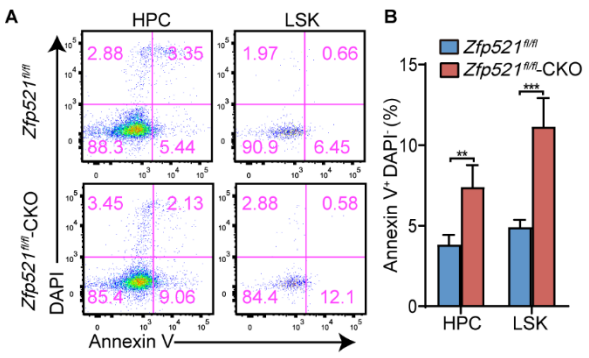

Figure S3. Frequencies of apoptosis remains increased in *Zfp521*-CKO chimeric mice at 4 month post-transplantation. Related to Figure 3.

(**A, B**) Flow cytometry images showing apoptosis in HPC and LSK cells obtained from *Zfp521*$^{fl/fl}$ and *Zfp521*-CKO chimeric mice at 4 month post-transplantation (**A**). The apoptotic profile of cells are presented on (**B**) Data are representative of three experiments (**A**) or are obtained from three experiments (**B**; mean ± SD of *n* = 7 mice per genotype) ***P* <0.01, ****P* <0.001 (Student's t test).

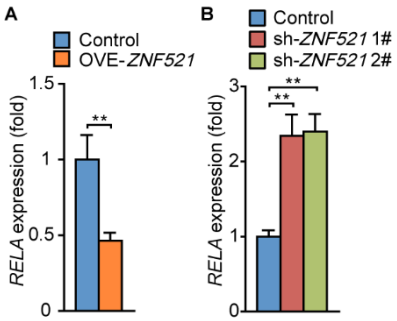

Figure S4. Zfp521 negatively regulated the expression of *RELA* in 293T cells. Related to Figure 7.

(**A, B**) Quantitative RT-PCR analysis of *RELA* mRNA in 293T cells with *ZNF521* overexpression (**A**) or knockdown (**B**); *ACTB* was used as the internal control and results are presented relative to those of 293T cells transfected with control vector. Data are from three independent experiments and are presented as mean ± SD. ***P* <0.01(Student's t test in **A**, one way analysis of variance with Bonferroni post-tests in **B**).

Table S1: Blood cell count in *Zfp521*-CKO and *Zfp521*$^{fl/fl}$ mice. Related to Figure 1.

	Zfp521$^{fl/fl}$	**Zfp521-CKO**	**p Value**
WBC (K/µL)	10.46±1.10	10.80±0.97	NS
NE (K/µL)	0.97±0.12	0.87±0.45	NS
LY (K/µL)	8.60±1.01	9.28±0.75	NS
MO (K/µL)	0.49±0.21	0.57±0.10	NS
EO (K/µL)	0.13±0.11	0.05±0.005	NS
BA (K/µL)	0.05±0.04	0.01±0.01	NS
Platelets (K/µL)	693.14±259.45	681.57±233.38	NS
RBC (M/µL)	10.34±1.29	9.90±0.84	NS
Hb (g/dL)	115.71±14.59	115±7.85	NS

Table S2: Blood cell count in *Zfp521*-CKO and *Zfp521*$^{fl/fl}$ chimeric mice. Related to Figure S2.

	Zfp521$^{fl/fl}$	**Zfp521-CKO**	**p Value**
WBC (K/µL)	13.5±2.52	13.43±1.98	NS
NE (K/µL)	13.5±0.64	6.71±0.67	NS
LY (K/µL)	7.36±1.63	7.39±1.91	NS
MO (K/µL)	0.81±0.22	0.57±0.26	NS
EO (K/µL)	0.24±0.05	0.32±0.08	NS
BA (K/µL)	0.07±0.01	0.13±0.03	NS
Platelets (K/µL)	806±135.91	734.33±94.99	NS
RBC (M/µL)	10.82±2.09	10.89±0.86	NS
Hb (g/dL)	124.75±19.15	126±3.56	NS

Table S3. Gene lists in the heatmap. Related to Figure 6.

Symbol	WT-1	WT-2	WT-3	KO-1	KO-2	KO-3	FoldChange	p value
Rela	4.168627432	4.260982514	3.797220911	9.680284075	9.215165111	10.15379403	5.607470784	5.20E-05
Xbp1	5.204428627	4.389972165	4.797220911	10.42307182	9.99424338	10.4570111	5.494234867	3.88E-05
Ube2q1	3.391205292	3.260982514	4.319160701	8.942051619	9.252499986	8.984862166	5.402688421	9.94E-05
Ogdh	4.06504348	4.102045987	4.527456577	9.662942149	9.281250781	9.699858405	5.316501764	1.19E-05
Pex7	3.981455489	3.689972165	4.812248369	9.184203608	9.275646637	9.833481746	5.269885322	0.000178347
Ndc80	4.924927712	4.260982514	4.448681132	8.889622911	9.440234055	10.93101307	5.20875956	0.001247411
Vkorc1	5.212982213	5.389972165	6.187923195	11.4571169	10.34105161	10.23752084	5.081603924	0.000496979
Zfp930	3.642922058	3.389972165	4.148124447	8.352078299	7.980068083	9.750853133	4.967326948	0.001043207
Tanc2	4.038898563	3.260982514	3.797220911	8.64168523	8.049591511	8.882249541	4.825474764	0.000139355
Uhmk1	5.783310783	5.741955961	6.038063419	9.562947942	10.52408035	11.38801908	4.637239067	0.00097605
Frs2	4.391205292	6.638401561	5.197944418	8.521276021	9.60054824	10.45425676	4.116176584	0.008842414
Tnpo3	5.991585986	5.015489716	6.096866645	8.676101991	9.809374703	10.65248365	4.011339332	0.003872837
Cetn3	7.813615107	6.835532328	6.810720594	11.03993978	10.50996687	11.90400047	3.998013033	0.001579485
mt-Nd4l	7.636724261	6.534354991	7.986772086	9.804231045	10.57365996	11.70826812	3.309435929	0.009358371
Csnk1e	5.839427974	6.400024079	7.538948506	8.81087195	9.996701961	10.73402517	3.254399506	0.012308485
Ctdsp1	7.693312076	6.741955961	7.316863446	9.810240714	9.942808837	10.85919515	2.953371074	0.002362582
Cdca3	9.854177392	8.260982514	8.173086207	11.85117514	10.82195124	11.8629664	2.749282223	0.013107222
Rhob	6.015455583	6.389972165	6.97121057	9.484347501	9.017671622	9.026751777	2.717377527	0.001027956
Ccnd1	8.270677038	7.102045987	9.257315976	10.07772542	11.22901362	11.37460099	2.683767009	0.022791946
Lypla1	7.434304267	6.665609033	8.094100112	9.100289796	9.864430904	10.96177578	2.577494357	0.019249661
Fam111a	7.285192633	6.524130639	8.46998609	9.306953427	9.729539573	10.88167617	2.546286601	0.025845424
Ppp3ca	8.333741492	7.260982514	8.569401641	10.16108786	9.467162644	11.67088692	2.378337259	0.035917447
Map4	4.887462112	3.835532328	5.178157315	6.838484721	7.798919042	5.962199643	2.232817217	0.028909862
Mpc2	9.389737418	7.516271628	9.180483165	10.52132852	10.53805709	11.6439668	2.205620065	0.034407055
Junb	7.071766002	8.303021642	7.827425704	9.87754136	9.45824218	10.0064367	2.046668963	0.006590129
Saa2	5.678329425	5.842920265	5.159414287	7.37499639	7.14076161	7.859570046	1.898221357	0.003012621
mt-Nd4	12.53342299	11.96131586	12.23898719	13.59114219	13.30474699	14.14715188	1.436438341	0.008460178
Fam25c	2.391205292	3.102045987	2.312471904	3.692453684	3.973779619	4.3181939	1.39290134	0.010818634
mt-Atp6	12.51162886	12.39890101	11.22025395	13.25292815	13.7129367	13.1842698	1.33978361	0.0395364
mt-Atp8	10.60271681	9.662389779	10.79794479	11.14333343	11.90363375	11.83694994	1.273621911	0.040510696
Spcs1	10.86247429	11.01818054	10.91965236	11.60296124	11.94754981	12.69266238	1.147622077	0.024152027
Tuba1a	12.16456366	11.44846511	10.65084575	9.933119639	10.34520504	9.905129396	-1.36014015	0.041618104
Dnmt1	10.517526	11.47788255	11.58251002	9.045618145	10.02666083	9.97095062	-1.51156299	0.031320652
Rps19-ps6	13.13631773	12.87415514	13.71343066	10.52148626	11.43104295	12.36252666	-1.80294922	0.037134861
Atf7ip	9.830727929	11.3912812	10.48503204	8.597476543	8.143208942	9.521940611	-1.81480502	0.040476971
Rap1b	12.83760873	13.08722253	13.13394433	11.68432884	11.49443535	10.37121514	-1.83626542	0.011942734
Zfand6	11.13180904	12.17888634	11.43474071	9.90561156	10.12752711	9.190933328	-1.8404547	0.01188104
Trim30a	11.49747717	13.09341461	11.55137417	10.03123868	10.83809681	9.714721014	-1.85273648	0.040594426
Ptp4a2	12.87336751	13.24012057	12.54635353	10.68589357	11.32129687	11.08636683	-1.85542812	0.002449835

Polb	9.780085747	11.65483796	11.48052811	9.380107768	8.847552404	8.760635712	-1.97571865	0.03473842
Ccz1	10.39870904	11.03340981	10.29081837	8.957887161	8.600090034	8.217165634	-1.98259813	0.003266776
Stambpl1	9.045755176	10.0557549	9.224203936	7.563697174	6.811444458	7.537287136	-2.13776175	0.005749806
Zyx	11.19323021	12.88938151	12.03154197	10.12453887	9.653424934	9.872703196	-2.15449557	0.013270332
Nsmce3	10.48647376	11.76998016	11.37995507	8.977338135	9.056942803	8.811570251	-2.26351927	0.004250645
Adgrg3	8.881455489	10.19560738	9.143029833	7.52442777	6.948035451	6.767729606	-2.32663329	0.007298107
Sfpq	11.57691075	12.08785122	11.77403452	9.766928457	9.099525379	9.352083274	-2.40675313	0.000601298
Cdkn1c	7.812431695	7.02607473	7.527456577	5.846301062	5.914218059	6.5450328	-1.35347036	0.013356189
Cenpe	10.94945601	11.52566727	10.62026394	8.13749617	8.649068804	8.514341746	-2.59816017	0.001050868
Rbms1	9.007757524	8.432065875	9.073977158	5.386127389	7.179652857	6.130705431	-2.60577163	0.009562989
Ssbp1	10.98162032	11.26923565	11.42384888	8.748687884	9.923957076	7.047407787	-2.6515507	0.03491685
Knl1	10.79684548	11.98175554	10.04481891	8.023611425	8.206979082	8.422791399	-2.72334601	0.00908765
Ier5	9.97930256	11.75908428	11.69423787	8.801952979	8.733880335	7.618260684	-2.75951024	0.016748875
Zfp260	10.04020097	8.000805235	8.451728068	6.584650473	5.595985491	5.422791399	-2.9631023	0.014435186
Chmp3	10.89195072	12.45601979	11.56418581	9.111231399	8.192004538	8.661656978	-2.98242114	0.004739453
Ubr2	10.71993972	11.42761213	11.37133875	8.446153163	8.996701961	7.09948563	-2.99218328	0.007901542
Tial1	9.573696136	10.04889096	10.27473732	7.708177837	6.026718413	6.962199643	-3.06674284	0.004386445
Smim3	10.74419696	11.13667149	9.621195163	7.227571913	7.495857926	7.422791399	-3.11861413	0.002493154
Ckap4	11.64782653	12.56389029	11.03120859	8.210540424	8.355751637	9.306745835	-3.12329584	0.005148857
Vps39	9.728272715	10.98090042	10.01573337	7.208887031	7.671525539	6.422791399	-3.14056751	0.003944768
Apoh	11.56381787	12.95351613	10.03806342	7.402054861	8.748588881	8.913922873	-3.16361027	0.03089474
Adipor1	11.2351641	13.44046797	12.85138999	10.02702269	9.329989958	8.661656978	-3.16945081	0.014536356
Chd9	10.74156782	11.66868413	11.46137261	8.851677104	8.161217915	7.3181939	-3.18017854	0.003746855
Csde1	11.21340109	12.62677586	12.2802064	8.806102798	10.26160816	6.937248747	-3.37180788	0.032734067
Vim	11.89904515	12.31975886	10.19031404	9.738711723	7.450312044	7.09948563	-3.37353622	0.032779056
Aplp2	10.69909222	12.89360776	12.23935899	8.851481965	9.480440766	7.353909003	-3.38207574	0.020248303
Ccdc127	11.08085626	12.58752704	11.38531426	8.638197962	8.397681253	7.353909003	-3.55463645	0.004211285
Rbm27	11.80116806	11.28702417	11.05628205	7.924980602	7.727752035	7.747731785	-3.58133662	9.75E-05
Wrn	9.820700437	10.97804837	9.57502528	7.48564172	6.048678899	6.004658125	-3.61159845	0.005164257
mt-Tt	6.853506325	9.924892006	7.226653449	4.713221336	4.93569992	3.422791399	-3.64444638	0.027640271
Krtdap	8.758309405	8.479668623	10.24202726	5.475693292	4.952257308	5.767729606	-3.76144169	0.003237691
Hist1h2bm	7.771777841	8.961028868	7.924856467	4.198227926	5.14579353	3.962199643	-3.78381403	0.00189422
Atp8b4	9.661518622	11.09303603	9.204935867	5.106988666	6.201837505	6.993379431	-3.88576164	0.007902702
Uvrag	9.65705529	10.85492358	11.77648391	7.010384438	6.765864495	6.422791399	-4.02980748	0.003191079
Pogz	7.967314809	8.652502482	8.910035474	3.920524341	4.609329161	3.422791399	-4.52573596	0.000523621
Ccr2	10.61643874	11.88504749	10.28286645	6.290651085	6.423001526	5.11965848	-4.98368053	0.001467651

Table S4. Antibody list. Related to Figures 2, 3, 4, 5, 7 and Figures S1, S2, S3.

Marker	Cat.NO.	Clone	Fluor	Vendor
Gr-1	108404	RB6-8C5	Biotin	Biolegend
TER-119	116204	TER-119	Biotin	Biolegend
B220	103204	RA3-6B2	Biotin	Biolegend
CD19	115504	eBio1D3 (1D3)	Biotin	Biolegend
IgM	408903		Biotin	Biolegend
IL-7R	135006	A7R34	Biotin	Biolegend
CD3	100304	eBio500A2 (500A2)	Biotin	Biolegend
Streptavidin	405208		APC-Cy7	Biolegend
Streptavidin	405226		BV421	Biolegend
Streptavidin	405205		PE-Cy5	Biolegend
Sca-1	108108	D7	PE	Biolegend
Sca-1	108105	D7	FITC	Biolegend
c-kit	105826	ACK2	APC-Cy7	Biolegend
CD48	103441	HM48-1	BV605	Biolegend
CD48	103424	HM48-1	PE-Cy7	Biolegend
CD150	115929	TC15-12F12.2	BV510	Biolegend
CD150	115927	TC15-12F12.2	BV605	Biolegend
CD150	115910	TC15-12F12.2	APC	Biolegend
c-kit	105812	ACK2	APC	Biolegend
CD16/32	101318	93	PE-Cy7	Biolegend
CD34	152208	RAM34	BV421	Biolegend
Ki-67	11-5698-82	SolA15	FITC	eBioscience
CD45.1	110708	A20	PE	Biolegend
CD45.2	109806	104	FITC	Biolegend
CD135	46-1351-82	A2F10	PerCP-eFluor710	eBioscience
Gr-1	108408	RB6-8C5	PE	Biolegend
TER-119	116212	TER-119	APC	Biolegend
CD71	113808	R17217 (RI7 217.1.4)	PE	Biolegend
B220	103208	RA3-6B2	PE	Biolegend
IgM	406509	II/41	APC	Biolegend
CD4	100408	GK1.5	PE	Biolegend
CD8a	100712	53-6.7	APC	Biolegend
AnnexinV	640941		APC	Biolegend

Table S5. Primers used in this study. Related to Figures 1, 6, 7 and Figures S4.

Primer names	Primer sequences (5'-3')
mZfp521 genotyping	
mZfp521-GT -F	GCTTGCCACGGCCTTATCTACTTTT
mZfp521-GT -R	CAACACGTTGGCTCACACTACT
Cre genotyping	
Cre-GT-F1	AGCGATGGATTTCCGTCTCTGG
Cre-GT-R1	AGCTTGCATGATCTCCGGTATTGAA
mZfp521 deletion	
mZfp521-del-F	GAAGACTTTTGGTCTGCAGAATTGCC
mZfp521-del-R	CAACACGTTGGCTCACACTACT
mZfp521-RT-PCR	
mZfp521-qPCR-F	CATGCCCAGAATCAGTCCCTC
mZfp521-qPCR-R	TTTGCACTCATGGTTCAGC
hZNF521-RT-PCR	
hZNF521-qPCR-F	CAAGCGAAACCGAGATCCCT
hZNF521-qPCR-R	CTTCCAACTCCTCCCCGTCT
mRela-RT-PCR	
mRela -qPCR-F	TATTGCTGTGCCTACCCGAAA
mRela -qPCR-R	TATTGCTGTGCCTACCCGAAA
hRELA-RT-PCR	
hRELA-qPCR-F	CTGCAGTTTGATGATGAAGA
hRELA-qPCR-R	TAGGCGAGTTATAGCCTCAG
mP16-RT-PCR	
mP16-qPCR-F	GGTTCTTGGTCACTGTGAGGA
mP16-qPCR-R	GCAGAAGAGCTGCTACGTGAA
mP21-RT-PCR	
mP21-qPCR-F	TGACCCACAGCAGAAGAG
mP21-qPCR-R	ACCAGCCTGACAGATTTCTA
mP27-RT-PCR	
mP27-qPCR-F	TGGACCAAATGCCTGACTC
mP27-qPCR-R	GGGAACCGTCTGAAACATTTTC
mP57-RT-PCR	
mP57-qPCR-F	CAGGACGAGAATCAAGAGCAG
mP57-qPCR-R	CGACGCCTTGTTCTCCTG
mActin-RT-PCR	
mActin-qPCR-F	ACCTTCTACAATGAGCTGCG
mActin-qPCR-R	CTGGATGGCTACGTACATGG
hActin-RT-PCR	
hActin-qPCR-F	GCACAGAGCCTCGCCTT
hActin-qPCR-R	GTTGTCGACGACGAGCG

pGL3-RelA-promoters	
pGL3-RelA-1229+252F	ATAgctagcTGGGCCATCTCTCCAGCCTG
pGL3-RelA-1229+252R	ATActcgagGCCCGTCGTCGCGTCACTGC
pGL3-RelA-496+252F	ATAgctagcCGGTGTGACCCTAGCTGGTT
pGL3-RelA-496+252R	ATActcgagGCCCGTCGTCGCGTCACTGC
pGL3-RelA-125+252F	ATAgctagcAGCCCTGGCTCGGCTCCAGT
pGL3-RelA-125+252R	ATActcgagGCCCGTCGTCGCGTCACTGC
pGL3-RelA+56+252F	ATAgctagcCGCGCTGCGGAGCTTGTAGT
pGL3-RelA+56+252R	ATActcgagGCCCGTCGTCGCGTCACTGC
Plove-Zfp521-3xFlag	
hZNF521-CDS -F	ATAgtcgacATGTCTCGCCGCAAGCAAGC
hZNF521-CDS-R	ATAcaattgACTGCTGTGTTGGGTCATTG
shZNF521-1#	
shZNF521-1#-F	CCGGGCTAAAGATAGTAATGCATTCTC
	GAGAATGCATTACTATCTTTAGCTTTTTG
shZNF521-1#-R	AATTCAAAAAGCTAAAGATAGTAATG
	CATTCTCGAGAATGCATTACTATCTTTAGC
shZNF521-2#	
shZNF521-2#-F	CCGGGCCCTCACTCTATAACCTAAACTC
	GAGTTTAGGTTATAGAGTGAGGGCTTTTTG
shZNF521-2#-R	AATTCAAAAAGCCCTCACTCTATAACCTAA
	ACTCGAGTTTAGGTTATAGAGTGAGGGC
shRela-1#	
shRela-1#-F	CCGGGGAGTACCCTGAAGCTATAACCTCG
	AGGTTATAGCTTCAGGGTACTCCTTTTTG
shRela-1#-R	AATTCAAAAAGGAGTACCCTGAAGCTATAA
	CCTCGAGGTTATAGCTTCAGGGTACTCC
shRela-2#	
shRela-2#-F	CCGGGCTCAAGATCTGCCGAGTAAACTCG
	AGTTTACTCGGCAGATCTTGAGCTTTTTG
shRela-2#-R	AATTCAAAAAGCTCAAGATCTGCCGAG
	TAAACTCGAGTTTACTCGGCAGATCTTGAGC
ChIP Seq binding site1	
Site-1-F	TGGGCCATCTCTCCAGCCTG
Site-1-R	GGTCCTCACATGAACCACTTGT
ChIP Seq binding site2	
Site-2-F	AGGACCAATGATGGCTGTGTGC
Site-2-R	TTCTGAATTGCTTTCCCAGGCT
ChIP Seq binding site3	
Site-3-F	AGCCTGGGAAAGCAATTCAGAA
Site-3-R	GCCATCTAAGCCAAGGGCAGGT

Transparent Methods

Mice and blood cell count

Zfp521$^{fl/fl}$ (B6, CD45.2) mice were generated by Cyagen (Suzhou, China). *Mx1-Cre* mice were purchased from Jackson Laboratory. *Zfp521*$^{fl/fl}$ were bred with Mx1-Cre mice to generate *Zfp521*-CKO mice. Mx1-Cre expression was induced by three intraperitoneal injections of poly(I:C) (GE Healthcare, Chicago, IL, USA) at a dosage of 8–10 mg/kg every second day. Peripheral blood samples were obtained by tail vein sampling into tubes containing EDTA. Complete blood count of peripheral blood was analyzed using Hemavet950FS (Drew Scientific, Dallas, TX, USA). Both male and female mice at 8–12 weeks of age were used for the experiments. Both 8- to 10-week-old female and male CD45.1 mice were used as recipients for all transplantation assays. All mice experiments were approved by the Animal Committee of the Institute of Zoology of the Third Military Medical University.

Flow cytometry

Flow cytometric analysis and cell sorting were performed as previously described with minor modifications (Hou et al., 2015a; Hou et al., 2015b). Single-cell suspensions were obtained from bone marrow (BM, flushed from tibias and femurs), peripheral blood , spleen, and thymus. Red cells were extracted using red blood cell lysis buffer (Solarbio Life Science, Beijing, China). The total cell number of BM obtained from two tibias and femurs of each mouse was counted with the TC20 automated cell counter (Bio-Rad, Hercules, CA, USA), and the cell numbers of hematopoietic stem and progenitor cells (HSPC) were based on the cellularity of total BM cells, multiplied by indicated frequencies of HSPC determined by flow cytometry. Unless stated otherwise, all antibodies were purchased from BioLegend (San Diego, CA, USA). All antibodies are listed in **Table S4**. For HSPC staining, BM cells were stained with a biotin lineage cocktail of anti-Ter-119, anti-B220, anti-Gr-1, anti-CD19, anti-CD3, anti-IgM, and anti-CD127. The following anti-mouse monoclonal antibodies were used for staining of cell surface markers: Streptavidin-APC-eFluor780, anti-Sca-1-PE, anti-c-Kit-APC, anti-CD16/32-PE-Cy7, anti-CD34-BV421, anti-Flt3-PerCP-eFluro710 (eBioscience, San Diego, CA, USA), anti-CD48-BV605, anti-CD150-BV510, for analysis of HSC, LT-HSC, ST-HSC, MPP, LSK cells, CD34^{-}LSK cells, HPC, lymphoid-primed multipotent progenitors, CMP, GMP, and MEP; anti-B220-PE and anti-IgM-APC, for analysis of B cells; anti-Gr-1-PE and anti-Mac-1-APC, for analysis of myeloid cells; anti-CD4-PE and anti-CD8-APC, for analysis of T cells; anti-CD71-PE and anti-Ter119-APC, for analysis of erythroid cells; anti-CD45.1-PE and anti-CD45.2-FITC, for distinguishing between donor and recipient cells.

For cell cycle analysis, 4 × 10^6 BM cells stained for HSC and progenitor cells were fixed and permeabilized with Cytofix/perm Kit (BD Pharmingen, San Diego, CA, USA) following the manufacturer's instructions. Cells were then stained with anti-ki67-FITC antibody (eBioscience) for 2 h at 4°C, before being stained with 4′,6-diamidino-2-phenylindole (DAPI) (8 μg/mL) overnight. For quiescent HSC sorting, BM cells were stained with pyronin Y (1μg/mL) and Hoechst33342 (1μg/mL) for 90 min and then stained with anti-Sca-1-FITC, anti-c-Kit-APC,

Streptavidin-APC- eFluor780, anti-CD48-PE-Cy7, and anti-CD150-BV605. For detecting apoptosis, BM cells stained for progenitor cells were stained with anti-annexinV-APC and DAPI in a binding buffer with Ca^{2+}. For caspase activity assay, the generic caspase activity assay kit for live cells (Beyotime Biotechnology, Shanghai, China) was used to detect the activities of caspase-3/7 in HSPCs according to the instructions of the manufacturer. BD CantoII Plus (BD Biosciences, San Jose, CA, USA) was used for fluorescence-activated cell sorting acquisition and Arial SORP for cell sorting. Flow cytometric analysis was done by gating on single cells and dead cells were excluded by DAPI or 7-AAD staining. Data was analyzed using FlowJo Version 10 software (TreeStar, Ashland, OR, USA).

Colony-forming unit assays

First, 6×10^4 BM mononuclear cells from *Zfp521*$^{fl/fl}$ or *Zfp521*-CKO mice were plated in 35-mm culture dishes with M3434 methylcellulose complete media (StemCell Technologies, Vancouver, BC, Canada), and incubated for 10–12 days at 37°C in 5% CO_2. On the last day, colonies were viewed with an inverted microscope. Discrete clusters containing >100 cells were considered to be colonies. For replating, colonies were washed and resuspended in PBS, 5×10^3 cells were plated into dishes with fresh M3434 media, and the process was repeated up to three generations.

Bone marrow transplantation assays

For competitive serial bone marrow transplantation assays, 2.5×10^6 BM cells from *Zfp521*$^{fl/fl}$ and *Zfp521*$^{fl/fl}$-CKO were mixed with 2.5×10^6 competitor BM cells ($CD45.1^+CD45.2^+$) and transplanted into lethally irradiated (9.5 Gy, Co^{60}) congenic $CD45.1^+$ recipient mice. For the second transplantation, 2×10^6 BM cells were transplanted to a second set of lethally irradiated mice.

5-FU treatment

Mice were administered 3 intraperitoneal injections of 5-fluorouracil (5-FU; 150 mg/kg) at 7 days intervals, and monitored for survival.

BrdU incorporation assay

In vivo BrdU incorporation was performed by intraperitoneally injecting 100 µL of 10 mg/mL BrdU (Sigma-Aldrich, St. Louis, MO, USA) into mice. Mice were sacrificed 12 hours after injection, and BM cells were harvested for further analysis. BM cells were stained with HSPC surface markers, and stained with BrdU using a BrdU Flow Kit (BD Pharmingen) per the manufacturer's instructions. Briefly, BM cells were fixed and permeabilized with Cytofix/Cytoperm buffer, digested with DNaseI, and stained with anti-BrdU-FITC antibody and DAPI (8 µg/mL) at 4°C overnight. The samples were analyzed using a BD CantoII Plus (BD Biosciences).

Homing assay

20×10^6 BM cells from *Zfp521*$^{fl/fl}$ or *Zfp521*$^{fl/fl}$-CKO mice were stained with 3 µM carboxyfluorescein succinimidyl ester (CFSE) (Invitrogen, Carlsbad, CA, USA) in 1 mL PBS at 37°C for 15 min, before an equal volume of pre-warmed fetal bovine serum was added to

terminate labeling. Cells were washed twice with PBS, before being retro-orbitally injected into the lethally irradiated (9.5 Gy, Co^{60}) recipient mice. BM cells were collected 6 h after injection, stained with lineage specific antibodies and anti-Sca-1-APC antibody, and the frequency of donor-derived cells was identified by fluorescence-activated cell sorting for $CFSE^+$ cells in $Lin^-Sca\text{-}1^+$ population.

RNA-Seq

Total RNA was purified from HSC isolated from *Zfp521*$^{fl/fl}$ or *Zfp521*-CKO mice with an RNeasy Micro Kit (Qiagen, Duesseldorf, Germany). The SMART-Seq v4 Ultra Low Input RNA Kit (Takara, Tokyo, Japan) was used to generate high-quality cDNA. Sequencing was performed commercially by Genergy Biotechnology (Shanghai, China), using an Illumina HiSeq X Ten instrument. The sequenced reads were aligned to the mouse genome (UCSC mm9) using Bowtie, with one mismatch allowed. Sequencing results were normalized to ERCC spike-in, and differentially expressed genes were characterized using DESeq2 (Version 1.26.0). Adjusted *P*-values were calculated by the Benjamini-Hochberg method. GSEA was performed with GSEA v2.0 software (Broad Institute, Cambridge, MA, USA).

RNA extraction and quantitative RT-PCR analysis

Total RNA was isolated with RNAiso plus (Takara) or an RNeasy Mini Kit (Qiagen) according to the manufacturer's instructions. cDNA was obtained using the PrimeScript RT Reagent Kit (Takara). Then, cDNA was subjected to real-time PCR using *Premix Ex Taq* II (Takara) and a Real-Time PCR Detection System (Bio-Rad). All primers are listed in **Table S5**. Experiments were performed in triplicate. Results were analyzed with the $2^{-\Delta\Delta Ct}$ method, and *Actb* was used for sample normalization.

ChIP assay

ChIP assay was performed using Magna ChIP HiSens Chromatin Immunoprecipitation Kit (Merck Millipore, Billerica, MA, USA) per the manufacturer's instructions. Briefly, *Zfp521*$^{fl/fl}$ or *Zfp521*$^{fl/fl}$-CKO mice were treated with one intraperitoneal injection of 5-FU at a dose of 150 mg/kg. BM cells were harvested 5 days post-injection, fixed for 10 min at 25°C with 1% formaldehyde, before excess formaldehyde was quenched with 125 mM glycine, by swirling for 5 min at room temperature. Cells were washed twice with pre-cooled PBS and were lysed in Nuclei Isolation Buffer with Protease Inhibitor Cocktail III for 15 min on ice. After cell lysis, crosslinked chromatin was sheared with a sonicator (SCIENTZ-IID, Scientz, Ningbo, China). Then, 5 μg anti-*Zfp521*(Abcam, Cambridge, MA, USA), 2 μg anti-H3K9 3me (Cell Signaling Technology, Danvers, MA, USA), 2 μg anti-H3K9-ac (Cell Signaling Technology), or IgG control were used for immunoprecipitation. DNA was eluted with ChIP Elution Buffer with 1 μL Proteinase K from precipitated immunocomplexes and subjected to quantitative real-time PCR analysis with the indicated primers (**Table S5**), for amplifying the binding region of *Zfp521*, H3k9 3me, and H3K9-ac in the NF-κB promoter region. ChIP enrichment was performed using the relative standard curve method of qPCR analysis to compare DNA from a mock IP vs. DNA immunoprecipitated using a specific ChIP antibody.

Luciferase reporter assay

The putative promoter of *Rela* was identified through sequence alignments with the promoter of *RELA* in humans. The putative promoter was amplified by PCR from mouse genomic DNA, which was digested with NheI and XhoI and cloned into a pGL3-Basic luciferase reporter vector. Three truncated fragments of the *Rela* promoter were cloned into a pGL3-Basic vector in the same way. For luciferase assays, 293T cells were split into 48-well plates in advance. Each pGL3-Basic vector, with full-length or truncated promoters, was transfected at 400 ng into 293T cells, together with 10 ng of pRL-TK. Cells were harvested 24 h after transfection and luciferase activities were assessed using a dual-luciferase reporter assay system per the manufacturer's instructions (Beyotime Biotechnology).

Lentiviral constructs and packaging

To generate the *ZNF521*- and *Rela*-specific shRNA plasmids, *ZNF521* and *Rela*-specific shRNA sequences were synthesized, and annealed and inserted into the pLKO.1 plasmid (#8453, Addgene) or pLKO.1-puro-CMV-TuroboGFP plasmid, which contains a TurboGFP-encoding gene that controlled by the CMV promoter.

Lentivirus production was performed as described before with minor modifications(Li et al., 2019). 293T cells were transfected with the *Rela* shRNA and lentiviral packaging plasmid psPAX2 (#12260, Addgene) and pMD2.G (#12259, Addgene) using polyethylenimine (Polysciences, Warrington, PA, USA). After 48 h incubation, the supernatants were collected and filtered through 0.45 μm filters, and concentrated by ultracentrifugation at 100,000 ×*g* for 3 h at 4°C. Virus pellets were resuspended in fresh medium, and stored at −80°C until use.

Lentiviral infection of BM cells

Zfp521$^{fl/fl}$ or *Zfp521*-CKO mice were treated with 5-FU five days prior to BM harvest. BM cells were incubated overnight in RPMI1640 with 10 ng/mL IL-3, 10 ng/mL IL-6, and 50 ng/mL SCF. Cells were incubated with concentrated lentiviral expressing *Rela*-specific shRNA and GFP on plates coated with RetroNectin (Takara), and spun for 2 h at 1000 ×*g*. Two rounds of spinfection were conducted, and cells were injected retro-orbitally into lethally irradiated 8-week-old recipient mice.

Western blot analysis

Protein extracts (50 μg) from Lin$^-$ BM cells were separated by 12% SDS-PAGE and then transferred onto 0.45-μm PVDF membranes (GE healthcare). Primary antibodies were incubated with the membranes overnight at 4°C. The membranes were washed in TBST (Solarbio Life Science) 3-5 times, incubated with the indicated HRP-conjugated secondary antibody (Beyotime Biotechnology) for 1 h at room temperature, and then washed in TBST 3-5 times. The signals were detected using an Immobilon Forte Western HRP substrate system (Merck Millipore).

Statistical analysis

All data are presented as the mean ± SD. Plots shown are representative of at least three independent biological replicates unless specifically indicated in the figure legends. Student's t-test was used when comparing two groups. One-way or two-way analysis of variance with

Bonferroni post-hoc test was performed for comparison among multiple populations. Differences in survival in either mice or patients was determined by log-rank test. Statistical analysis was performed using GraphPad Prism 6 (GraphPad Prism, La Jolla, CA, USA). For all analyses, a *P*-value of <0.05 was considered statistically significant.

Supplemental References

Hou, Y., Li, W., Sheng, Y., Li, L., Huang, Y., Zhang, Z., Zhu, T., Peace, D., Quigley, J.G., Wu, W*., et al.* (2015a). The transcription factor Foxm1 is essential for the quiescence and maintenance of hematopoietic stem cells. Nat Immunol *16*, 810-818.

Hou, Y., Wang, X., Li, L., Fan, R., Chen, J., Zhu, T., Li, W., Jiang, Y., Mittal, N., Wu, W*., et al.* (2015b). FHL2 regulates hematopoietic stem cell functions under stress conditions. Leukemia *29*, 615-624.

Li, Z., Li, H., Xu, X., Wang, L., Liu, B., Zheng, W., Lian, L., Song, Y., Xia, X., Hou, L*., et al.* (2019). Haploinsufficiency of GCP4 induces autophagy and leads to photoreceptor degeneration due to defective spindle assembly in retina. Cell death and differentiation.